Theoretical Models of Exchange Interactions in Dimeric Transition-Metal Complexes

A. Ceulemans,* L. F. Chibotaru, G. A. Heylen, K. Pierloot, and L. G. Vanquickenborne

Laboratory of Quantumchemistry, University of Leuven, Celestijnenlaan 200 F, B-3001 Belgium

Received April 12, 1999

Contents

1. Introduction

Dinuclear complexes of transition-metal ions are important molecular models for magnetic materials. They have been studied extensively both from an experimental and a theoretical point of view. A broad survey of the literature is presented in the monograph by Kahn.[1] Several reviews[2−5] and feature articles highlight the potential use of molecular magnets as magnetic materials, and comprehensive model treatments of exchange coupling through the first transition series continue to appear.[6−10] From a theoretical point of view, the Heisenberg−Dirac−Van Vleck Hamiltonian occasionally combined with simple molecular orbital calculations has certainly dominated the field, ever since the seminal 1959 paper by Anderson[11,12] on the theory of superexchange interactions. Only quite recently has this situation started to change when detailed ab initio methods were developed which make the direct calculation of exchange levels possible. Progress is dependent on the complementarity of the two approaches. The model treatment without reliable quantitative calculations is empty since it provides a formal framework of parametric energy expressions which cannot be used unless the parameters are known. On the other hand, the ab initio calculations without the model are blind since they lack concepts which bring order and insight in the manifold of calculated levels. The harmonious combination of both approaches has now been realized for a number of highly symmetric dimers of $(t_{2g})^n$ transition-metal ions, and this will form the main message which this review tries to transmit.

* Corresponding author.

2. The Spin Hamiltonian

The preferential vehicle of magnetochemists and magnetophysicists for the study of molecular magnetism is the spin Hamiltonian formalism. This formalism is based on an effective spin−spin coupling operator which incorporates the interactions between the magnetic sites. Especially when combined with additional Zeeman terms, it constitues—in the words of Griffith—"a convenient resting place" in the physical landscape between experiment and theory.[13] One may admire its invaluable synthetic power to reduce a large set of experimental data to only a few empirical coupling constants but should also note a possible drawback: it may indeed convey the false impression that the coupling between sites is of magnetic origin, while it is actually due to the usual kinetic and potential energy terms of the underlying molecular Schrödinger equation. Spin Hamiltonians thus always call for a microscopic theory of weak exchange interactions. As we will show, such theories are currently being implemented for dimer complexes. For larger spin clusters though the call remains largely unanswered.[14]

For a good understanding of the theoretical basis of spin Hamiltonians, here we will follow the opposite path and reconstruct the famous Anderson model of exchange coupling starting from a simple microscopic theory of two interacting sites with one magnetic orbital on each. In spite of its simplicity, the model will render considerable services when constructing Hamiltonians in more complicated cases, discussed in the following sections. Let A and B be the sites and ϕ^A and ϕ^B the respective orbitals. These orbitals will be assumed to be of Wannier type, which means that they are localized as much as possible while keeping orthonormality.[15] Orbital transformations will be expressed by creation and annihilation operators,[16] such as $a_\alpha^\dagger$, which creates an electron with α spin in $|\phi^A\rangle$ or b_β, which destroys an electron with β spin in $|\phi^B\rangle$. The number operator $n_\alpha^A = a_\alpha^\dagger a_\alpha$ counts the number of electrons with α spin (1 or 0) in $|\phi^A\rangle$,

10.1021/cr960129k CCC: $35.00
Published on Web 01/22/2000

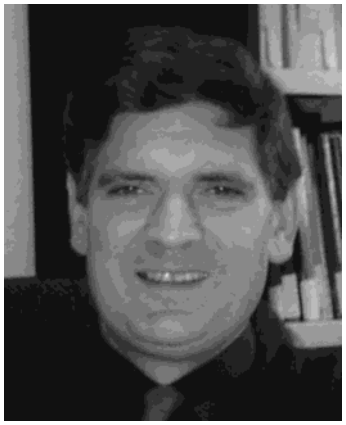

Arnout Ceulemans is a Professor at the Department of Chemistry, University of Leuven. He received his Ph.D. and Dr. Hab. degrees in Leuven, and teaches Group Theory, Chemical Physics, and Inorganic Chemistry. His main research interests are the applications of group-theoretical and topological methods at the border between chemistry and physics.

Liviu F. Chibotaru a is Research Fellow at the Department of Chemistry, University of Leuven. He received his Ph.D. degree in theoretical physics from the Academy of Sciences in Kishinev, Moldova. His current interests include electron correlation and vibronic interactions in extended systems.

etc. The Hamiltonian for this system contains both intrasite and intersite terms:

$$H = H_0^A + H_0^B + H_0^{AB} + V$$

$$H_0^A = U n_\alpha^A \, n_\beta^A$$

$$H_0^B = U n_\alpha^B \, n_\beta^B$$

$$H_0^{AB} = U' \sum_{\sigma,\sigma'} n_\sigma^A \, n_{\sigma'}^B + \sum_{\sigma,\sigma'} a_\sigma^\dagger \, b_{\sigma'}^\dagger a_{\sigma'} b_\sigma$$

$$V = t \sum_\sigma (a_\sigma^\dagger b_\sigma + b_\sigma^\dagger a_\sigma) \qquad (1)$$

The parameter U represents the Coulombic repulsion between two electrons on the same site, while U' is the repulsion between electrons on different sites. B is a genuine exchange parameter corresponding to the matrix element $\langle \phi^A(1)\phi^B(2)|1/r_{12}|\phi^A(2)\phi^B(1)\rangle$. The term V symbolizes the *transfer term* which originates from the interaction between the equisymmetric orbitals on the two sites. The corresponding parameter t represents the one-electron matrix element between the two orbitals. Occupation of the two orbitals by two electrons yields three singlet states

Goedele A. Heylen completed her Ph.D. study on the "Theoretical analysis of exchange interactions in face-sharing bioctahedral complexes of Ti(III), Cr(III), and Co(II)" at the division of Quantum Chemistry, University of Leuven. She is currently employed at Massive Industries.

Kristine Pierloot is a Research Director of the Flemish Science Foundation, working at the Department of Chemistry, University of Leuven, where she also received her Ph.D. Her main interest is the application of ab initio methods for the study of spectroscopic and magnetic properties of transition-metal systems.

Luc G. Vanquickenborne is a Professor of theoretical chemistry at the Department of Chemistry, University of Leuven. He received his Ph.D. and Dr. Hab. in Leuven, where he teaches Quantum Chemistry, Computational Chemistry, and Inorganic Chemistry. His main research interests are in the application of computational methods in different areas of chemistry.

and one triplet state. A basis which diagonalizes $H_0 = H_0^A + H_0^B + H_0^{AB}$ corresponds to the eigenstates $|\Phi_k^0\rangle$ with energies $E_k (k = 1 - 4)$ listed in Table 1 $|\Phi_1^0\rangle$ and $|\Phi_2^0\rangle$ are so-called 'covalent' states with one electron on each site, while the remaining $|\Phi_3^0\rangle$ and

Table 1. Eigenstates of the Zeroth-Order Hamiltonian

$\lvert\Phi_1^0\rangle = \frac{1}{\sqrt{2}}(\phi^A(1)\phi^B(2) + \phi^A(2)\phi^B(1))$	$\frac{1}{\sqrt{2}}(\alpha_1\beta_2 - \alpha_2\beta_1)$	$U' + B$
$\lvert\Phi_2^0\rangle = \frac{1}{\sqrt{2}}(\phi^A(1)\phi^B(2) - \phi^A(2)\phi^B(1))$	$\begin{cases}\alpha_1\alpha_2\\ \frac{1}{\sqrt{2}}(\alpha_1\beta_2 + \alpha_2\beta 1)\\ \beta_1\beta_2\end{cases}$	$U' - B$
$\lvert\Phi_3^0\rangle = \phi^A(1)\phi^A(2)$	$\frac{1}{\sqrt{2}}(\alpha_1\beta_2 - \alpha_2\beta_1)$	U
$\lvert\Phi_4^0\rangle = \phi^B(1)\phi^B(2)$	$\frac{1}{\sqrt{2}}(\alpha_1\beta_2 - \alpha_2\beta_1)$	U

$|\Phi_4^0\rangle$ are of the 'ionic' type with double occupation on one site. The transfer term connects $|\Phi_1^0\rangle$ to the ionic states. A dinuclear complex is of the exchange or Heisenberg[17] type, as opposed to the bond or Hückel type, if the transfer integral t is much smaller than the repulsion between two electrons on the same center. In this case the covalent states will determine the ground state and low-lying excited states of the system. For these states the transfer term acts as a perturbation which can be incorporated into an effective Hamiltonian by means of a unitary transformation. One defines an operator S in the space of H_0 eigenstates

$$S = \sum_{k,l} \frac{V_{kl}}{E_k - E_l} |\Phi_k^0\rangle \langle\Phi_l^0| \tag{2}$$

where V_{kl} is the matrix element $\langle\Phi_k^0|V|\Phi_l^0\rangle$. The unitary transformation of H by S is given by ref 18

$$\begin{aligned}\tilde{H} = e^S He^{-S} = \\ \left(1 + S + \frac{1}{2}S^2 + ...\right)(H_0 + V)\left(1 - S + \frac{1}{2}S^2 - ...\right) \\ = H_0 + V + [S, H_0] + [S, V] + \\ \frac{1}{2}[S, [S, H_0]] + ...\end{aligned} \tag{3}$$

with

$$[S, V] = \sum_{k,n}\left\{\sum_l \left(\frac{1}{E_k - E_l} + \frac{1}{E_n - E_l}\right) V_{kl}V_{ln}\right\}|\Phi_k^0\rangle\langle\Phi_n^0| \tag{4}$$

Upon substitution this result simplifies to

$$\tilde{H} = H_0 + \frac{1}{2}[S, V] + ... \tag{5}$$

When working out the expression for the commutator, we may neglect the small exchange contribution of B in the denominators. The transfer term in $\tilde{H}$ then becomes

$$\frac{1}{2}[S, V] = -\frac{2t^2}{U - U'}\sum_\sigma (n_\sigma^A\, n_{-\sigma}^B - a_\sigma^\dagger\, b_{-\sigma}^\dagger\, b_\sigma a_{-\sigma}) \tag{6}$$

This effective Hamiltonian splits the covalent states as

$$\text{Triplet} \quad |\Phi_2^0\rangle:\ U' - B$$

$$\text{Singlet} \quad |\Phi_1^0\rangle:\ U' + B - \frac{4t^2}{U - U'} \tag{7}$$

The electrostatic exchange parameter B, which is bound to be positive since it represents a self-repulsion of a charge cloud, will favor the triplet state, while the transfer term will invariably stabilize the singlet state through second-order interaction with the high-lying ionic states which are also singlets. The microscopic treatment thus leads to a simple prediction that the spin ordering of the ground state is determined by the interplay of exchange and transfer interactions. The exchange interactions promote a ferromagnetic ordering, while the transfer contributions lead to antiferromagnetic ordering. In the Anderson terminology, the exchange part is referred to as the *potential* energy part since it derives from the Coulomb operator while the transfer interaction is the *kinetic* part since it is due to the hopping of an electron from one site to the other. We now introduce local spin operators $\boldsymbol{S}_A$ and $\boldsymbol{S}_B$. These act selectively on spin orbitals which are localized on the corresponding site. Their components (in units of $\hbar$) can easily be expressed as follows

$$\begin{aligned}2S_A^z &= n_\alpha^A - n_\beta{}^A \\ 2S_A^x &= a_\alpha^\dagger a_\beta + a_\beta^\dagger a_\alpha \\ 2S_A^y &= -ia_\alpha^\dagger a_\beta + ia_\beta^\dagger a_\alpha\end{aligned} \tag{8}$$

and similarly for $\boldsymbol{S}_B$. Note that the total spin operator corresponds to the sum $\boldsymbol{S} = \boldsymbol{S}_A + \boldsymbol{S}_B$. One further has

$$2\boldsymbol{S}_A\cdot\boldsymbol{S}_B = \sum_\sigma \left(\frac{1}{2}n_\sigma^A\, n_\sigma^B - \frac{1}{2}n_\sigma^A\, n_{-\sigma}^B + a_\sigma^\dagger a_{-\sigma} b_{-\sigma}^\dagger b_\sigma\right) \tag{9}$$

Using this expression, the effective Hamiltonian in eq 5 can be converted into a constant term and a spin−spin coupling term. The associated coupling parameter in the Heisenberg−Dirac−Van Vleck terminology is denoted as $-2J$

$$\tilde{H} = \left(U' - \frac{B}{2} - \frac{t^2}{U - U'}\right)n^A n^B - 2\, J\, \boldsymbol{S}_A\cdot\boldsymbol{S}_B$$

with

$$J = B - \frac{2t^2}{U - U'} \tag{10}$$

where $n^A = n_\alpha^A + n_\beta^A$ and similarly for n^B. The spin−spin coupling term can easily be evaluated from

$$2\boldsymbol{S}_A\cdot\boldsymbol{S}_B = \boldsymbol{S}^2 - \boldsymbol{S}_A^2 - \boldsymbol{S}_B^2$$

and equals $-3/2$ for the singlet and $+1/2$ for the triplet. The gap between triplet and singlet thus amounts to $-2J$. A negative J parameter corresponds to a singlet ground state and thus is characteristic of antiferromagnetic coupling.

This explicit derivation of the spin Hamiltonian paradigm illustrates several important points. First of all it is immediately clear that the spin operators do not play any physical role. They only appear because they are practical tools to discriminate the two spin states concerned. One could equally well use

a symmetry element in orbital space which interchanges sites A and B, say $\hat{\sigma}|\phi^A\rangle = |\phi^B\rangle$. In the context of the covalent states, $\hat{\sigma}$ may be written as

$$\hat{\sigma} = \sum_{\sigma\sigma'} b_\sigma^\dagger a_{\sigma'}^\dagger b_{\sigma'} a_\sigma \tag{11}$$

The equivalence between $\hat{\sigma}$ and $\boldsymbol{S}_A\cdot\boldsymbol{S}_B$ reads

$$\hat{\sigma} = -2\boldsymbol{S}_A\cdot\boldsymbol{S}_B - \frac{1}{2} n^A n^B \tag{12}$$

The singlet $|\Phi_1^0\rangle$ and triplet $|\Phi_2^0\rangle$ functions are, respectively, symmetric and antisymmetric with respect to this spatial symmetry element and thus can equally well be discriminated by orbital symmetry. Alternatively, one could also replace the spin operators by the exchange operator P^{AB} which switches the local spins. The Dirac identity[19] expresses this operator as

$$P^{AB} = 2\boldsymbol{S}_A\cdot\boldsymbol{S}_B + \frac{1}{2} n^A n^B \tag{13}$$

From these expressions, the product of both operators is found to be equal to minus the identity operator

$$P^{AB}\hat{\sigma} = -1 \tag{14}$$

This close link between orbital and spin exchange is nothing other than the Pauli exclusion principle: exchanging both spins and orbitals corresponds to permuting electrons and will change the sign of the wave function. In problems with many orbitals per site, such as transition-metal centers with five active d orbitals on each metal, this connection between spin and orbital exchange is not so tight and generalizations of the spin Hamiltonian formalism are thus far from obvious. Nonetheless, in the literature, one did not hesitate to apply the spin−spin coupling formalism in these cases as well. As an early example, in the discussion of the optical spectra of manganese pairs, Ferguson et al.[20] introduced a Hamiltonian of the type

$$\tilde{H}_{ex} = -2\sum_{ij} J_{A_iB_j}\, \boldsymbol{S}_{A_i}\cdot\boldsymbol{S}_{B_j} \tag{15}$$

where i and j run over all magnetic orbitals. Kahn[21] issued a warning that this Hamiltonian is not invariant under unitary transformations of the orbital basis and should not be used. The proper alternative is to develop a microscopic theory for the case of multiorbital sites. This approach has now been carried out for a number of highly symmetric bioctahedral complexes of $(t_{2g})^n$ metal ions, as will be reviewed in the next sections.

A final caveat concerns the confrontation of the Anderson parametrization scheme with ab initio results. An approach which was popular during the early days of semiempirical methods and continues to be used in the DFT-type calculations is the so-called frozen orbital approach. It tries to determine an optimal set of orbitals from which all relevant states may be calculated. From this set the one-electron and two-electron parameters which appear in the model Hamiltonian may be determined by direct calculation. At the correlated level of calculation, this frozen orbital approach breaks down. Indeed, the correlated wave function may be a convolution of millions of determinants from which the kinetic and potential parts, which contribute to the ferromagnetic gap, can no longer be separated. The decomposition of J in Coulomb and transfer contributions remains useful though when comparing exchange splittings in a series of analogous compounds with varying intercenter distance.

For degenerate systems, a single-molecule calculation yields much more information because of the large numbers of eigenstates. Several parameters can then be extracted by inverting the parametric expressions for the calculated eigenvalues. In ideal high-symmetry cases, this confrontation may lead to a single consistent coupling scheme of the entire exchange manifold. The challenges for the theoretical description thus mainly concern the study of exchange interactions for magnetic ions with unquenched orbital moments. The cases we will consider are the ideal ones with tetragonal and trigonal symmetry.

3. Exchange Interactions between Orbitally Degenerate Ions: Tetragonal Symmetry

In this section we examine the exchange interactions in orbitally degenerate transition-metal ions in a linear oxo-bridged geometry. There are a number of specific features of this vertex-shared bioctahedral geometry which simplify the theoretical expressions: (i) a high idealized tetragonal symmetry, D_{4h} or D_{4d}, which yields a highly specific state labeling, (ii) long M−M distances which imply that the two-electron interaction integrals between the centers are very small, (iii) strong axial crystal fields which separate the dimer states into relatively isolated configurational manifolds.

In recent years Weihe and Güdel published a number of interesting studies of the linear and bent oxo-bridged dimers[8,22−24] which were based on a consistent extension of the Anderson model. Recently Tsukerblat et al.[9] presented a much more formal account of this approach making use of tensor algebra.

Here we will present a simplified version of the d^1-d^1 case which is entirely taken from the first draft of ref 8 but in the final paper was replaced by the more complicated d^2-d^2 system.

The d^1-d^1 case is exemplified in complexes with a Ti(III)−O−Ti(III) core. The D_{4h} geometry is shown in Figure 1. The parametrization scheme includes ligand-field and transfer interactions: the transfer for the $d_{xy}^A-d_{xy}^B$ pair is denoted as δ, while $d_{xz}^A-d_{xz}^B$ and $d_{yz}^A-d_{yz}^B$ interactions are parametrized as $-\pi$. Δ_t measures the tetragonal splitting of the t_{2g} shell as $\Delta_t = E(d_{xz},d_{yz}) - E(d_{xy})$. The covalent states of

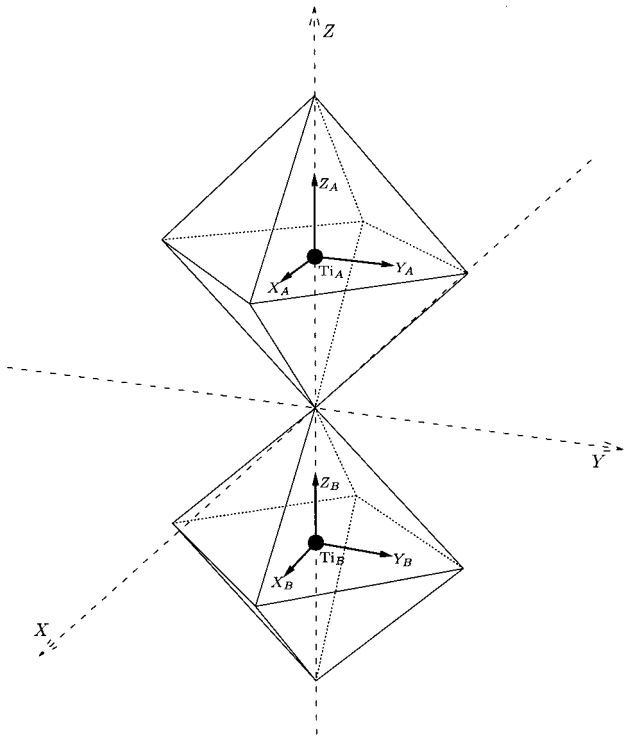

Figure 1. Cartesian frame for the vertex-shared bioctahedral Ti dimer.

$t_{2g}^1-t_{2g}^1$ are separated by the tetragonal field in three manifolds with D_{4h} labels as follows:

$$d_{xy}^1 - d_{xy}^1: {}^3A_{2u}, {}^1A_{1g}$$

$$d_{xy}^1 - (d_{xz}, d_{yz})^1: {}^3E_u, {}^3E_g, {}^1E_g, {}^1E_u$$

$$(d_{xz}, d_{yz})^1 - (d_{xz}, d_{yz})^1: {}^3A_{2u}, {}^3A_{2g}, {}^3B_{1u}, {}^3B_{2u}, {}^1A_{1g}, {}^1A_{1u}, {}^1B_{1g}, {}^1B_{2g} \quad (16)$$

The ionic or charge-transfer states of $t_{2g}^2-t_{2g}^0$ derive from t_{2g}^2 octahedral parent states ${}^3T_{1g}$, ${}^1E_g$, ${}^1T_{2g}$, and ${}^1A_{1g}$. The dimer states originating from these parents and split by the tetragonal field are presented in the following scheme:

$$\begin{aligned}
{}^3T_{1g} \quad & {}^3E \nearrow \ {}^3E_g, {}^3E_u : U_1 = U - \tfrac{1}{3}\Delta_t \\
& {}^3A_2 \searrow \ {}^3A_{2g}, {}^3A_{1u} : U_2 = U + \tfrac{2}{3}\Delta_t \\
{}^1E_g \quad & {}^1A_1 \nearrow \ {}^1A_{1g}, {}^1A_{2u} : U_3 = U + 6B + 2C - \tfrac{2}{3}\Delta_t \\
& {}^1B_1 \searrow \ {}^1B_{1g}, {}^1B_{2u} : U_5 = U + 6B + 2C + \tfrac{2}{3}\Delta_t \\
{}^1T_{2g} \quad & {}^1E \nearrow \ {}^1E_g, {}^1E_u : U_4 = U + 6B + 2C - \tfrac{1}{3}\Delta_t \\
& {}^1B_2 \searrow \ {}^1B_{2g}, {}^1B_{1u} : U_5 = U + 6B + 2C + \tfrac{2}{3}\Delta_t \\
{}^1A_{1g} \quad & \rightarrow \quad {}^1A_{1g}, {}^1A_{2u} : U_6 = U + 15B + 5C
\end{aligned}$$

In these expressions the ionic terms are spread out over six levels with energies $U_i (i = 1, 6)$ depending on Racah's interelectronic repulsion parameters B and C and the crystal-field splitting of the t_{2g} shell, Δ_t. The parameter U positions the lowest charge-transfer state ${}^3T_{1g}$ with respect to the d^1-d^1 configuration.

In Table 2 we reproduce the results of an Anderson-type parametrization from the work of Güdel and Weihe. Interestingly, for this geometry large-scale multireference calculations were performed by Fink et al.[25] In this study the bulky nonbridging ligands were replaced by He-like model ligands with charges that reproduce the spectroscopic strength of these complexes. The results are included in the table. The U_i parameters appear in the denominators of the kinetic terms, but no attempt was made to correct these further for the crystal-field splitting of the covalent states. When interpreting the results, it will be assumed that δ exchange between the d_{xy} orbitals is negligible in view of the absence of d-type valence orbitals on the bridging ligand. The exchange splitting is thus uniquely due to π exchange. Perhaps the most surprising feature of the resulting expression is that the charge-transfer pathways which control the kinetic part are almost uniquely defined by symmetry. Indeed, for all covalent states there is only one or no charge-transfer state of the same symmetry. The only exception occurs for the ${}^1A_{1g}$ states which are connected both to the ${}^1E_g$ and ${}^1A_{1g}$ octahedral parents. In this way a transparent set of expressions is obtained, which clearly shows how the relative ordering in a given manifold is entirely determined by the strengths of the U_i parameters in the denominators. As Weihe and Güdel emphasize, it is gratifying to see how well these qualitative trends are obeyed by the ab initio results.

Table 2. Exchange Manifold for d^1 Ions in Tetragonal Symmetry

	term	ab initio[a] [25]	first order	second order[8]
$(b_2)^1(b_2)^1$	${}^1A_{1g}$	0	0	$-4/3\ \delta^2/U_6 - 8/3\ \delta^2/U_3$
	${}^3A_{2u}$	0	0	0
$(b_2)^1(e)^1$	${}^3E_g$	5194	Δ_t	$-(\pi+\delta)^2/U_1$
	${}^3E_u$	5195	Δ_t	$-(-\pi+\delta)^2/U_1$
	${}^1E_g$	5238	Δ_t	$-(-\pi+\delta)^2/U_4$
	${}^1E_u$	5272	Δ_t	$-(\pi+\delta)^2/U_4$
$(e)^1(e)^1$	${}^3A_{2g}$	9940	$2\Delta_t$	$-4\pi^2/U_2$
	${}^1B_{2g}$	10279	$2\Delta_t$	$-4\pi^2/U_5$
	${}^1B_{1g}$	10287	$2\Delta_t$	$-4\pi^2/U_5$
	${}^1A_{1g}$	10580	$2\Delta_t$	$-8/3\pi^2/U_6 - 4/3\pi^2/U_3$
	${}^1A_{1u}$	11284	$2\Delta_t$	0
	${}^3B_{1u}$	11345	$2\Delta_t$	0
	${}^3B_{2u}$	11348	$2\Delta_t$	0
	${}^3A_{2u}$	11409	$2\Delta_t$	0

[a] In cm^{-1}.

In principle, these results should also form an important test case for the tensor formalism of ref 9. It must be noted though that the symmetry labels in ref 9 show systematic errors; the states originating from the $d_{xy}-d_{xy}$ configuration are wrongly labeled as ${}^1A_{1g}$ and ${}^3A_{1g}$ instead of ${}^1A_{1g}$ and ${}^3A_{2u}$, etc.... A detailed comparison is further prevented by quite different views on the role of ligand-field interactions in the two treatments: the results in Table 2 are to the first order determined by the large tetragonal splitting of the t_{2g} shell, but this effect is not considered in the tensor treatment of ref 9. In contrast, the latter formalism explicitly considers the less important onsite configuration interaction between $(t_{2g})^2$ and $(t_{2g})^1(e_g)^1$ terms in the ionic manifold. These different coupling conditions may affect the composition of the eigenvectors for states which are not uniquely defined by symmetry labels. This may limit the applicability of the tensor model.

In the discussion of exchange Hamiltonians, the present Anderson approach is often compared to the natural magnetic orbital (NMO) approach, which was proposed by several authors including Kahn.[1,26,27] In the latter approach, the basis orbitals are so-called natural orbitals that are completely localized on a given site, say $|f^A\rangle$ and $|f^B\rangle$. These orbitals are nonorthogonal, as opposed to the Wannier functions, $|\phi^A\rangle$ and $|\phi^B\rangle$, underlying the Anderson approach. Let S_{AB} be their overlap integral

$$\langle f^A|f^B\rangle = S_{AB} \tag{17}$$

A standard transformation relates the two sets of orbitals:

$$|\phi^A\rangle = \frac{1}{2}\left(\frac{1}{\sqrt{1+S_{AB}}} + \frac{1}{\sqrt{1-S_{AB}}}\right)|f^A\rangle + \frac{1}{2}\left(\frac{1}{\sqrt{1+S_{AB}}} - \frac{1}{\sqrt{1-S_{AB}}}\right)|f^B\rangle$$

$$|\phi^B\rangle = \frac{1}{2}\left(\frac{1}{\sqrt{1+S_{AB}}} - \frac{1}{\sqrt{1-S_{AB}}}\right)|f^A\rangle + \frac{1}{2}\left(\frac{1}{\sqrt{1+S_{AB}}} + \frac{1}{\sqrt{1-S_{AB}}}\right)|f^B\rangle \tag{18}$$

It is evident that energy calculations do not depend on transformations of the orbital basis and thus will yield exactly the same result, irrespective of the kind of basis orbitals that are used. Hence, it is not possible to have a conflicting interpretation due to a different choice of orbital basis.

A possible source of confusion is related to the definition of the NMO's. There is indeed no rigorous way to define the exact meaning of the term "localized".[1] If one is looking for a truly natural orbital basis, one could equally well take this concept to its limit and construct natural orbitals in such a way that the configuration interaction is completely quenched.[26] The antiferromagnetic ground state then corresponds to a pure Heitler−London-type exchange pair

$$\Psi = \frac{1}{\sqrt{2(1+S_{AB}^2)}}(|f_\alpha^A f_\beta^B| - |f_\beta^A f_\alpha^B|) \tag{19}$$

The same function in a Wannier basis reads

$$\Psi = \frac{a}{2}(|\phi_\alpha^A \phi_\beta^B| - |\phi_\beta^A \phi_\alpha^B|) + \frac{b}{2}(|\phi_\alpha^A \phi_\beta^A| + |\phi_\alpha^B \phi_\beta^B|) \tag{20}$$

The canonical set of natural magnetic orbitals which fulfills this requirement is given by

$$|f^A\rangle = \cos\varphi|\phi^A\rangle + \sin\varphi|\phi^B\rangle$$

$$|f^B\rangle = \cos\varphi|\phi^B\rangle + \sin\varphi|\phi^A\rangle$$

with

$$2\varphi = \arcsin b/a \tag{21}$$

In this basis the kinetic part of the exchange is entirely incorporated in the diagonal matrix elements. The price to pay is that one can no longer use a simple set of natural orbitals of this type to cover all the spectral states of a given manifold. This may be rather inconvenient and provides an important disadvantage of the NMO approach versus the Wannier-type approach.

4. Exchange Interactions between Orbitally Degenerate Ions: The d^1–d^1 Case in Trigonal Symmetry

4.1. The Exchange Hamiltonian from First Principles

As compared to the vertex-shared dimers, the face-shared binuclear complexes of transition metals with unquenched orbital moments present several new challenges: (i) short metal−metal distances which imply that the intercenter Coulomb terms cannot be neglected, (ii) concomitant through-bond and through-space transfer pathways for the t_{2g} orbitals, (iii) a small trigonal field which may be comparable to the exchange splitting. The prime paradigmatic case which has received much attention is the face-shared bioctahedral $Ti_2X_9^{3-}$ (X = Cl, Br) complex with trigonal symmetry.[28−30] This is a degenerate t_{2g}^1−t_{2g}^1 problem which lacks the extra complication of onsite Coulombic repulsion in the covalent states. A full microscopic theory of this problem has recently been developed.[31] We will use these results as a framework to review the existing model treatments.

The symmetry of the dimer is D_{3h}. Trigonal forms of the t_{2g} orbitals on each center are described as follows:

$$|a^A\rangle = d_{z^2}^A$$

$$|\theta^A\rangle = \frac{1}{\sqrt{3}}(d_{xz}^A + \sqrt{2}d_{x^2-y^2}^A)$$

$$|\epsilon^A\rangle = \frac{1}{\sqrt{3}}(d_{yz}^A - \sqrt{2}d_{xy}^A)$$

$$|a^B\rangle = d_{z^2}^B$$

$$|\theta^B\rangle = \frac{1}{\sqrt{3}}(-d_{xz}^B + \sqrt{2}d_{x^2-y^2}^B)$$

$$|\epsilon^B\rangle = \frac{1}{\sqrt{3}}(-d_{yz}^B - \sqrt{2}d_{xy}^B) \tag{22}$$

The d-orbital functions in this expression refer to the local Cartesian (x^A, y^A, z^A) and (x^B, y^B, z^B) frames shown in Figure 2.

The labels a, θ, and ϵ refer to the standard trigonal symmetry conventions.[32,33] Relative phases of the orbitals have been chosen in such a way that the horizontal symmetry plane, $\hat{\sigma}_h$, precisely interchanges corresponding orbitals on sites A and B.

$$\hat{\sigma}_h|a^A\rangle = |a^B\rangle$$

$$\hat{\sigma}_h|\theta^A\rangle = |\theta^B\rangle$$

$$\hat{\sigma}_h|\epsilon^A\rangle = |\epsilon^B\rangle \tag{23}$$

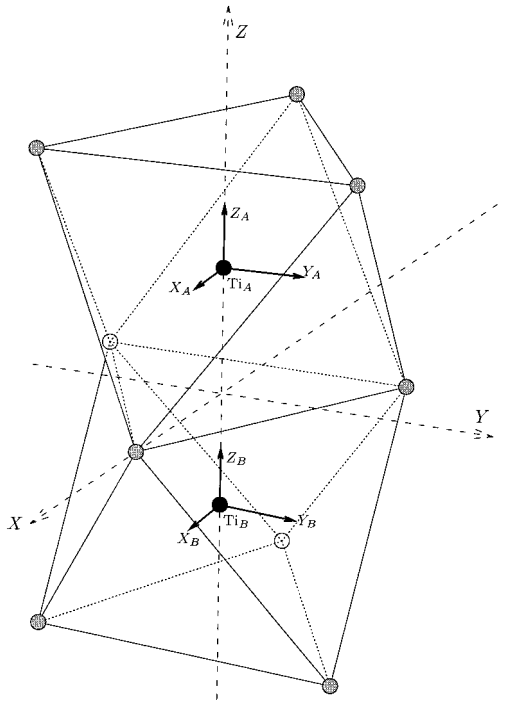

Figure 2. Cartesian frame for the face-shared bioctahedral Ti dimer.

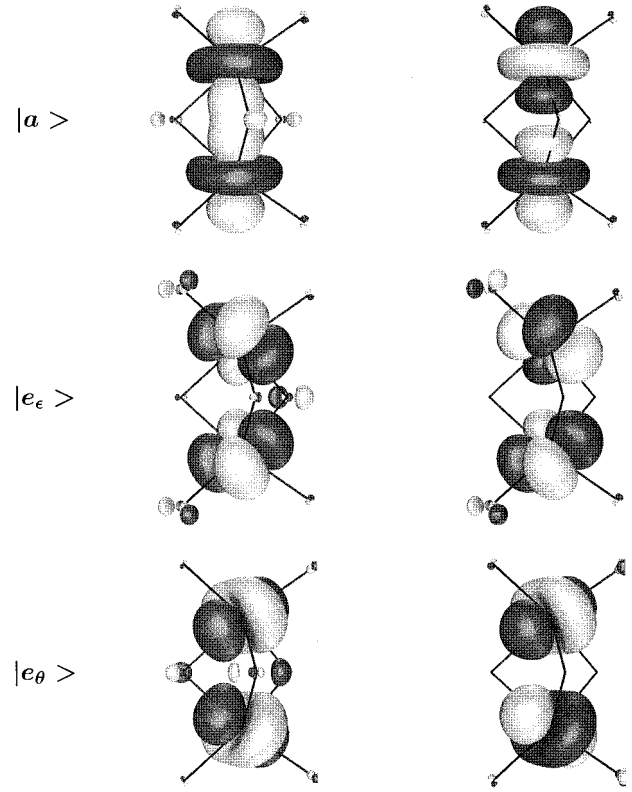

Figure 3. Contour plots of symmetric (left) and antisymmetric (right) molecular orbital combinations of the a and e basis orbitals. Note the π-antibonding Ti−Cl interactions in the e combinations. This feature indicates that the transfer between the e orbitals is accomplished via a superexchange pathway involving the bridging ligands. In contrast, transfer between the a orbitals is of the direct through-space type.

This element thus permutes orbitals at different sites. In Figure 3 we present contour plots of symmetric and antisymmetric molecular orbital contributions with dominant t_{2g} character. The real trigonal forms of the t_{2g} orbitals were described in detail in a study of the emitting doublet states in trigonal Cr(III) complexes.[32] As compared to the nondegenerate case, the creation and annihilation operators now receive an additional orbital label, $i = a, \theta, \epsilon$. Generalization of eq 1 for t_{2g} orbitals yields

$$H_0^A = U_{||} \sum_i n_{i\alpha}^A n_{i\beta}^A + U_\perp \sum_{i<j} \sum_{\sigma\sigma'} n_{i\sigma}^A n^A{}_{j\sigma'} - \frac{1}{2} J \sum_{i\neq j} \sum_\sigma (n_{i\sigma}^A n_{j\sigma}^A - a_{i\sigma}^\dagger a_{j\sigma} a_{i-\sigma}^\dagger a_{j-\sigma} - a_{i\sigma}^\dagger a_{j\sigma} a_{j-\sigma}^\dagger a_{i-\sigma}) + \Delta \sum_\sigma (n_{\epsilon\sigma}^A + n_{\theta\sigma}^A) \quad (24)$$

The Coulomb repulsion depends on whether the two electrons are in the same t_{2g} orbital ($U_{||}$) or in different t_{2g} orbitals ($U_\perp$). J is the exchange integral, and Δ measures the trigonal splitting of the t_{2g} shell. In a d-only formalism, the repulsion integrals obey the pseudospherical relationship

$$U_{||} - U_\perp = 2J \quad (25)$$

The intercenter two-electron interactions are described by

$$H_0{}^{AB} = \frac{1}{2} \sum_{\sigma\sigma'} \sum_{ijkl} (U_{ijkl}(a_{i\sigma}^\dagger b_{j\sigma'}^\dagger b_{l\sigma'} a_{k\sigma} + b_{i\sigma}^\dagger a_{j\sigma'}^\dagger a_{l\sigma'} b_{k\sigma}) + B_{ijkl}(a_{i\sigma}^\dagger b_{j\sigma'}^\dagger a_{l\sigma'} b_{k\sigma} + b_{i\sigma}^\dagger a_{j\sigma'}^\dagger b_{l\sigma'} a_{k\sigma})) \quad (26)$$

The explicit form of this Hamiltonian taking into account trigonal symmetry relations is given in Appendix 1. In the denominators of the subsequent unitary transformation, the B parameters are neglected and the U_{ijkl} parameters are reduced to a single isotropic repulsion parameter U'. The transfer term connects equisymmetric orbitals on the two centers and discriminates between a- and e-type exchange

$$V = t_a \sum_\sigma (a_{a\sigma}^\dagger b_{a\sigma} + b_{a\sigma}^\dagger a_{a\sigma}) \; t_e \sum_\sigma (a_{\theta\sigma}^\dagger b_{\theta\sigma} + a_{\epsilon\sigma}^\dagger b_{\epsilon\sigma} + b_{\theta\sigma}^\dagger a_{\theta\sigma} + b_{\epsilon\sigma}^\dagger a_{\epsilon\sigma}) \quad (27)$$

From here on the construction of the effective Hamiltonian runs precisely as indicated in section II. Resulting parametric energy expressions for the pair states of the $t_{2g}{}^1-t_{2g}{}^1$ configuration are listed in Table 3. In Figure 4 we represent a schematic energy level diagram to facilitate the further discussion.

The energy expressions provide a powerful analytical tool to rationalize experiment, ab initio calculations, and model treatments. We will summarize here the main results. The configurational averages of the

Table 3. Parametric Energy Expressions for the $(t_{2g})^1-(t_{2g})^1$ Configuration and CASPT2 Results in cm^{-1} [31]

$(a\times a)$	$^1A_1'$	$U_{aaaa}+B_{aaaa}-\frac{8t_a^2}{3(U_\parallel-U'-J+\frac{2}{3}\Delta)}-\frac{4t_a^2}{3(U_\parallel-U'+2J+\frac{4}{3}\Delta)}$	0
	$^3A_2''$	$U_{aaaa}-B_{aaaa}$	735
$(a\times e)$	$^1E''$	$\Delta+U_{a\theta a\theta}-U_{aa\theta\theta}+B_{a\theta\theta a}-B_{a\theta a\theta}-\frac{t_a^2+t_e^2-2t_at_e}{U_\parallel-U'-J}$	639
	$^3E''$	$\Delta+U_{a\theta a\theta}+U_{aa\theta\theta}-B_{a\theta\theta a}-B_{a\theta a\theta}-\frac{t_a^2+t_e^2-2t_at_e}{U_\parallel-U'-3J}$	673
	$^3E'$	$\Delta+U_{a\theta a\theta}-U_{aa\theta\theta}-B_{a\theta\theta a}+B_{a\theta a\theta}-\frac{t_a^2+t_e^2+2t_at_e}{U_\parallel-U'-3J}$	744
	$^1E'$	$\Delta+U_{a\theta a\theta}+U_{aa\theta\theta}+B_{a\theta\theta a}+B_{a\theta a\theta}-\frac{t_a^2+t_e^2+2t_at_e}{U_\parallel-U'-J}$	793
$(e\times e)$	$^3A_2'$	$2\Delta+U_{\theta\theta\theta\theta}-3U_{\theta\theta\epsilon\epsilon}-B_{\theta\theta\epsilon\epsilon}-2B_{\theta\epsilon\epsilon\theta}+B_{\theta\theta\theta\theta}-\frac{4t_e^2}{U_\parallel-U'-3J}$	1501
	$^1A_1''$	$2\Delta+U_{\theta\theta\theta\theta}-3U_{\theta\theta\epsilon\epsilon}+B_{\theta\theta\epsilon\epsilon}+2B_{\theta\epsilon\epsilon\theta}-B_{\theta\theta\theta\theta}$	1510
	$^3E''$	$2\Delta+U_{\theta\theta\theta\theta}-U_{\theta\theta\epsilon\epsilon}+B_{\theta\theta\epsilon\epsilon}-B_{\theta\theta\theta\theta}$	1531
	$^1E'$	$2\Delta+U_{\theta\theta\theta\theta}-U_{\theta\theta\epsilon\epsilon}-B_{\theta\theta\epsilon\epsilon}+B_{\theta\theta\theta\theta}-\frac{4t_e^2}{U_\parallel-U'-J}$	1531
	$^3A_2''$	$2\Delta+U_{\theta\theta\theta\theta}+U_{\theta\theta\epsilon\epsilon}-B_{\theta\theta\epsilon\epsilon}-B_{\theta\theta\theta\theta}$	1546
	$^1A_1'$	$2\Delta+U_{\theta\theta\theta\theta}+U_{\theta\theta\epsilon\epsilon}+B_{\theta\theta\epsilon\epsilon}+B_{\theta\theta\theta\theta}-\frac{4t_e^2}{3(U_\parallel-U'-J-\frac{4}{3}\Delta)}-\frac{8t_e^2}{3(U_\parallel-U'+2J-\frac{2}{3}\Delta)}$	1561
$(a\times a)-(e\times e)$	$^3A_2''$	$\sqrt{2}U_{aa\theta\theta}-\sqrt{2}B_{aa\theta\theta}$	
	$^1A_1'$	$\sqrt{2}U_{aa\theta\theta}+\sqrt{2}B_{aa\theta\theta}+2\sqrt{2}(\frac{t_at_e}{3(U_\parallel-U'-J-\frac{2}{3}\Delta)}+\frac{t_at_e}{3(U_\parallel-U'-J-\frac{4}{3}\Delta)}-\frac{t_at_e}{3(U_\parallel-U'+2J+\frac{4}{3}\Delta)}-\frac{t_at_e}{3(U_\parallel-U'+2J-\frac{2}{3}\Delta)})$	

crystal-field configurations $(a\times a)$, $(a\times e)$, and $(e\times e)$ are given by

$$E(a\times a)=-\frac{2t_a^2}{U_\parallel-U'}+U_{aaaa}$$

$$E(a\times e)=\Delta-\frac{t_a^2+t_e^2}{U_\parallel-U'}+U_{a\theta a\theta} \qquad (28)$$

$$E(e\times e)=2\Delta-\frac{2t_e^2}{U_\parallel-U'}+U_{\theta\theta\theta\theta}-U_{\theta\theta\epsilon\epsilon}$$

Leaving aside the U_{ijkl} parameters, the effective $a\rightarrow e$ promotion energy is thus equal to $\Delta-(t_e^2-t_a^2)/(U_\parallel-U')$. The anisotropy of the transfer term will thus contribute to the trigonal splitting. The diamagnetism of the $Ti_2Cl_9^{3-}$ ground state[29,34] strongly suggests that the $(a\times a)$ configuration is lowest, which implies a positive effective crystal-field splitting. Precise estimates of the splitting are difficult since correlation effects seem to play a dominant role. The antiferromagnetic gap of the ground configuration is on the order of 735 cm^{-1}. This is in good agreement with the temperature dependence of the magnetic susceptibility.[35] The gap is clearly due to a strong exchange interaction between the d_{z^2} obitals. The transfer term $4t_a^2/(U_\parallel-U')$ is probably on the order of 700−800 cm^{-1}.

In the excited $(a\times e)$ manifold at all levels of calculation, the states that are antisymmetric with respect to the site-permuting symmetry plane are lowest in energy. The separation between the averages of the symmetric ($^1E'$ and $^3E'$) and antisymmetric ($^1E''$ and $^3E''$) states is given by

$$\frac{1}{2}(^1E'+{}^3E')-\frac{1}{2}(^1E''+{}^3E'')=-2t_at_e\left(\frac{1}{U_\parallel-3J-U'}+\frac{1}{U_\parallel-J-U'}\right)+2B_{a\theta a\theta} \qquad (29)$$

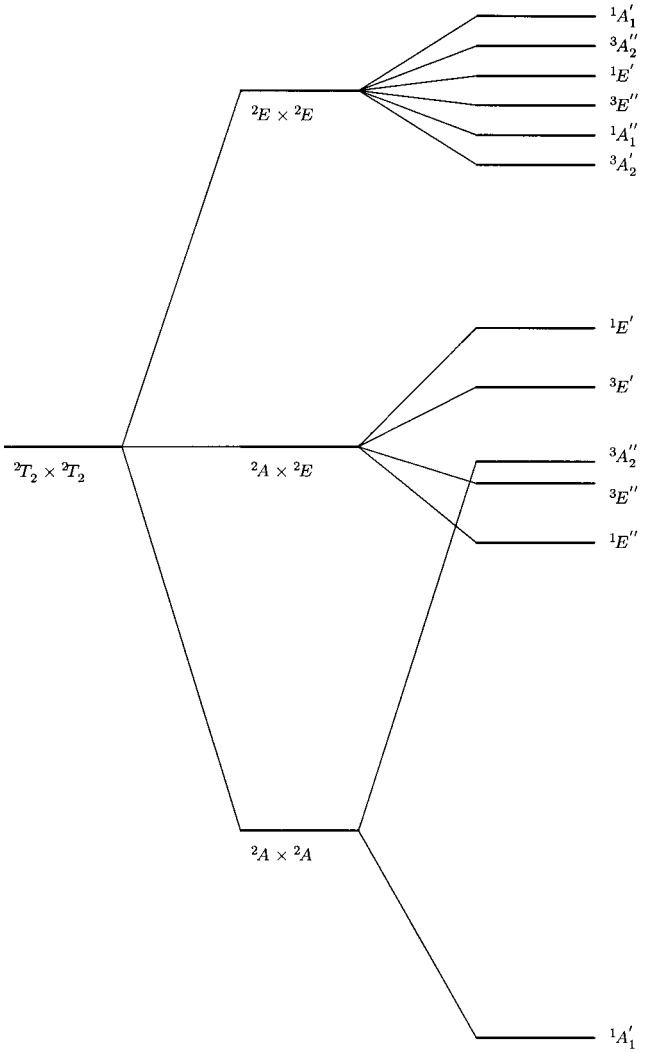

Figure 4. Schematic energy level diagram for the $t_{2g}^1-t_{2g}^1$ system in D_{3h} symmetry. (Reproduced with permission from ref 35. Copyright 1999 Taylor and Francis, London.)

This clearly resembles the Anderson result of eq 10, but in contrast to the nondegenerate case, the present gap law does not separate spin states but orbital

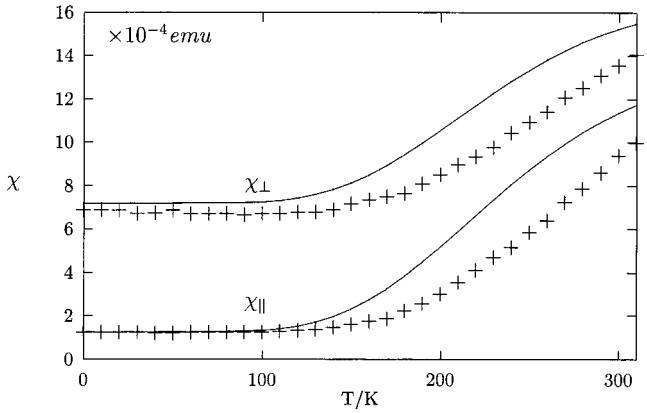

Figure 5. Calculated (full lines, $\zeta = 154$ cm^{-1}, $k = 0.75$) and experimental[29] susceptibility curves for $Ti_2Cl_9^{3-}$, corrected for atomic diamagnetism. (Reproduced with permission from ref 35. Copyright 1999 Taylor and Francis, London.)

symmetries. An exchange Hamiltonian based on the site-permutation operator is thus nearer to the exchange coupling phenomena than a spin−spin coupling Hamiltonian. To a first approximation with complete neglect of J and $B_{a\theta a\theta}$, the kinetic exchange coupling in the excited state, $4t_at_e/(U_{||} - U')$, equals -100 cm^{-1}. This implies a ratio of the transfer parameters as $t_a/t_e \approx -7$. This is an important result of the ab initio calculations. The orbital plots in Figure 2 clearly show that the exchange interaction between d_{z^2} orbitals is of the direct 'through space' type.[36] In contrast, the exchange between the e orbitals is of the superexchange 'through ligand'[37,38] type.

In the (e × e) manifold splittings are rather small. A consistent parametrization is possible under the assumption that only the U and B parameters are important. This yields $U_{\theta\theta\epsilon\epsilon} \approx 10$ cm^{-1} and both $B_{\theta\theta\theta\theta}$ and $B_{\theta\theta\epsilon\epsilon}$ on the order of 5 cm^{-1}. In summary, there is a clear hierarchical order of interactions, which we may schematically represent as follows:

$$\Delta - \frac{(t_e^2 - t_a^2)}{U_{||} - U'} \gtrsim \frac{4t_a^2}{U_{||} - U'} \gg \frac{-4t_at_e}{U_{||} - U'} \gg U_{iiii} > B_{iijj} \tag{30}$$

The calculated exchange spectrum has recently been compared to experimental susceptibility curves.[35] To this aim, spin−orbit and Zeeman interactions were introduced into the Hamiltonian. The results are reproduced in Figure 5. Note that the only adjustable parameters in this plot are the spin−orbit constant, ζ, and the orbital reduction factor, k.

Experimentally, three important pieces of information may be extracted from the data: (*i*) the temperature-independent anisotropy, (*ii*) the onset of the magnetization, and (*iii*) the curvature of the susceptibility rise. These relate to the nature of the electronic ground state in zero field, the energy gap to the first excited states, and the magnetic character of the states which are populated at higher temperature, respectively. Comparison between theory and experiment is very satisfactory in view of the fact that the ab initio results do not contain adjustable orbital parameters. The comparison can be easily made perfect by introducing a slight energy shift of the (a × e) states to higher energy and introduction of a small diamagnetic correction. On the other hand, it must be kept in mind that susceptibility curves do not yield the kind of detailed information that can be obtained by direct spectroscopy.

Very recently, Borrás-Almenar et al.[10] proposed an alternative explanation of the magnetic anisotropy in $Ti_2Cl_9^{3-}$. We include a brief discussion of this proposal in the subsequent section.

4.2. Comparison to Extended Spin Hamiltonians

In the past decades several models have been devoted to the $Ti_2X_9^{3-}$ problem. The widespread use of the spin Hamiltonian has inspired many authors to introduce additional angular momentum operators to cope with orbital degeneracy.[28−30,39] With the exception of the work by Tsukerblat et al.,[9] these studies did not make use of the powerful vector coupling techniques that were developed in atomic physics and could now render excellent services for the construction of molecular pair states. Instead, trial and error methods were preferred. These require a critical review.

The t_{2g} degeneracy is particularly favorable for a spherical analysis because of the $p-t$ isomorphism, which makes it possible to describe the t_{2g} components by a fictitious $L = 1$ angular momentum.[40] The $t_{2g}^1-t_{2g}^1$ problem does reduce in a spherical limit to a $^2P \times {}^2P$ atomic coupling model. Borrás-Almenar et al.[10] very recently pointed out that there are not one but two spherical limits with dramatically different magnetic behaviors. Both limits can be represented in the scheme of the model Hamiltonian. We must first examine the $p-t$ isomorphism on a two-center system in more detail. It can easily be verified that the matrix representation of a local angular momentum operator $\mathbf{L}^A$ in the t_{2g}^A basis is identical to the action of the angular momentum operator in a basis of p orbitals, provided the following identifications are made

$$|a^A\rangle \approx p_z$$
$$|\theta^A\rangle \approx p_x$$
$$|\epsilon^A\rangle \approx p_y \tag{31}$$

A similar mapping holds for the local $\mathbf{L}^B$ operator acting on the states of the t_{2g}^B orbitals but with a sign change for the z component

$$|a^B\rangle \approx -p_z$$
$$|\theta^B\rangle \approx p_x$$
$$|\epsilon^B\rangle \approx p_y \tag{32}$$

This sign change is a consequence of the fact that the orbital bases on the two centers were constructed as mirror images. The isomorphism implies that we can construct $t_{2g}^1-t_{2g}^1$ states by taking the coupled states of two inequivalent p electrons and then performing the appropriate substitutions as pre-

Table 4. Parametric Expressions for the t2g¹−t2g¹ Configuration under Spherical Symmetry Constraints[a]

	$-t_a = t_e$	$t_a = t_e$	
^1S	$(^1A_1')$	$(^1A_1')$	$U_{iiii} + B_{iiii} + 2(U_{iijj} + B_{iijj}) - \frac{4t^2}{U-U'+2J}$
^1P	$(^1A_1'', ^1E')$	$(^1A_1'', ^1E'')$	$U_{iiii} - B_{iiii} - 3(U_{iijj} - B_{iijj})$
^1D	$(^1A_1', ^1E', ^1E'')$	$(^1A_1', ^1E', ^1E')$	$U_{iiii} + B_{iiii} - (U_{iijj} + B_{iijj}) - \frac{4t^2}{U-U'-J}$
^3S	$(^3A_2'')$	$(^3A_2'')$	$U_{iiii} - B_{iiii} + 2(U_{iijj} - B_{iijj})$
^3P	$(^3A_2', ^3E'')$	$(^3A_2', ^3E')$	$U_{iiii} + B_{iiii} - 3(U_{iijj} + B_{iijj}) - \frac{4t^2}{U-U'-3J}$
^3D	$(^3A_2'', ^3E', ^3E'')$	$(^3A_2'', ^3E'', ^3E'')$	$U_{iiii} - B_{iiii} - (U_{iijj} - B_{iijj})$

[a] Levels are characterized as ^{2S+1}L states, together with their trigonal offspring. As explained in the text, there are two possible spherical limits which only differ by their eigenvector composition, as specified in eqs 33 and 34. We refer to these cases as $-t_a = t_e$ and $t_a = t_e$, respectively.

scribed by eqs 31 and 32. Our trigonal Hamiltonian can be adapted to this special limit by imposing the following relationships

$$\begin{gathered}\Delta = 0\\ t = -t_a = t_e\\ U_{iiii} = U_{aaaa} = U_{\theta\theta\theta\theta}\\ U_{iijj} = -U_{aa\theta\theta} = U_{\theta\theta\epsilon\epsilon}\\ U_{ijij} = U_{a\theta a\theta} = U_{\theta\epsilon\theta\epsilon} = U_{iiii} - 2U_{iijj}\\ B_{iiii} = B_{aaaa} = B_{\theta\theta\theta\theta}\\ B_{iijj} = -B_{aa\theta\theta} = B_{a\theta\theta a} = B_{\theta\theta\epsilon\epsilon} = B_{\theta\epsilon\epsilon\theta}\\ B_{ijij} = -B_{a\theta a\theta} = B_{\theta\epsilon\theta\epsilon} = B_{iiii} - 2B_{iijj}\end{gathered} \tag{33}$$

Note that all parameters which correspond to population of the $|a^B\rangle$ orbital by a single electron are accompanied by a minus sign as a result of the identification of $|a^B\rangle$ with a $-p_z$ component. Under these conditions, the eigenvalues are indeed grouped together in degenerate levels which formally may be assigned as the $^1S + {}^3S + {}^1P + {}^3P + {}^1D + {}^3D$ results of the $^2P \times {}^2P$ product, as shown in Table 4.

Of course we could also choose not to make the sign change, i.e., to identify the second p_z component directly with $|a^B\rangle$. The parameter relationships that will accomplish this are given by

$$\begin{gathered}\Delta = 0\\ t = t_a = t_e\\ U_{iiii} = U_{aaaa} = U_{\theta\theta\theta\theta}\\ U_{iijj} = U_{aa\theta\theta} = U_{\theta\theta\epsilon\epsilon}\\ U_{ijij} = U_{a\theta a\theta} = U_{\theta\epsilon\theta\epsilon} = U_{iiii} - 2U_{iijj}\\ B_{iiii} = B_{aaaa} = B_{\theta\theta\theta\theta}\\ B_{iijj} = B_{aa\theta\theta} = B_{a\theta\theta a} = B_{\theta\theta\epsilon\epsilon} = B_{\theta\epsilon\epsilon\theta}\\ B_{ijij} = B_{a\theta a\theta} = B_{\theta\epsilon\theta\epsilon} = B_{iiii} - 2B_{iijj}\end{gathered} \tag{34}$$

This leads to the same spherical levels but with an altered eigenvector composition, i.e., with $|a^B\rangle$ replaced by $-|a^B\rangle$. We want to stress that both coupling schemes are correct spherical limits of the trigonal system. Borrás-Almenar et al.[10] rightly point out that the Zeeman interactions in both limits will be quite different since the eigenvectors are not the same. The limit with $t_a = -t_e$ leads to isotropic Zeeman interactions, while the coupling limit with $t_a = t_e$ produces a highly anisotropic Zeeman effect. It is clear that the actual parametric regime, which was obtained by a comparison of the model expressions with ab initio results, is very far from either spherical symmetry.

The results in Table 4 are full of symmetries of different kinds. In the $t_a = t_e$ coupling scheme, the single prime states, which are symmetric under site exchange by the $\hat{\sigma}_h$ plane, carry an Anderson-type interaction with B_{iiii} as the potential part and a transfer term with varying denominators as the kinetic part. The total parity of these states, expressed as $(-1)^{S+L}$, is even. In contrast, the odd parity states, with $(-1)^{S+L} = -1$, have no kinetic part and $-B_{iiii}$ as the potential part. The denominators in the table can be approximated as follows

$$\frac{1}{U - U' + xJ} = \frac{1}{U - U'} - x\frac{J}{(U - U')^2} \tag{35}$$

Under this approximation, the kinetic part can entirely be absorbed in effective Coulomb parameters

$$\begin{aligned}\tilde{U}_{iiii} &= U_{iiii} - \frac{2t^2}{U - U'}\\ \tilde{B}_{iiii} &= B_{iiii} - \frac{2t^2}{U - U'}\\ \tilde{U}_{iijj} &= U_{iijj} - \frac{2Jt^2}{(U - U')^2}\\ \tilde{B}_{iijj} &= B_{iijj} - \frac{2Jt^2}{(U - U')^2}\end{aligned} \tag{36}$$

$\tilde{U}_{iiii}$ is a global shift parameter which only fixes the origin of energy. As a result, the general spherical Hamiltonian for the exchange interaction between two t_{2g} shells requires only three effective parameters: $\tilde{B}_{iiii}$, $\tilde{U}_{iijj}$, $\tilde{B}_{iijj}$. In this form it is equivalent to the coupling of two inequivalent p electrons in atomic physics, which is described by three Slater−Condon parameters. The Wigner−Racah coupling calculus is best suited to construct an appropriate effective Hamiltonian, using irreducible tensor operators.[41] Since the $\tilde{B}_{iiii}$ term only depends on the total parity, it will be a tensor quantity of zeroth rank. In contrast, the $\tilde{U}_{iijj}$ and $\tilde{B}_{iijj}$ parameters depend on L and are second-rank quantities. This order of interactions is in general agreement with our estimates of the

physical importance of the parameters. This implies that a correct spherical model may be a valid starting point for a description of the actual complex, provided the trigonal splitting is introduced in an appropriate way.

In the literature one often finds semiempirical Hamiltonians which were not based on such considerations but involve trial and error combinations of the invariants $\boldsymbol{S}_A\cdot\boldsymbol{S}_B$ and $\boldsymbol{L}_A\cdot\boldsymbol{L}_B$. An elaborate example is the study by Drillon and Georges[39] which uses only two effective parameters. When we compare their spectrum with the expressions in Table 4, correspondence is obtained if one omits U_{iiii}, U_{iijj}, and B_{iijj} and neglects the difference in the denominators for the ^1S and ^1D expressions so that these terms become degenerate. The latter assumption is quite artificial since a similar difference between the denominators for the ^1D and ^3P terms is maintained. It restricts the intraionic repulsion during charge transfer to a spin−spin coupling term. This is not an adequate description of the $(t_{2g})^2$ repulsion states, which appear in the denominators of the transfer terms.

Furthermore, when applying the Hamiltonian to the trigonal dimer, the French school puts the entire task of symmetry breaking in the hands of the crystal-field splitting parameter. In contrast, Leuenberger and Güdel,[30] who start off from a less sophisticated spherical limit, use Δ in conjunction with different hopping parameters for the *a* and *e* pathways. This choice was based on extended Hückel calculations and is corroborated by our analysis based on CASSCF results.

In summary, the development of a full-tensor Hamiltonian for the exchange between two $^2T_{2g}$ states requires a spherical parametrization scheme with zeroth and second-rank quantities as in the case of the coupling of two inequivalent p electrons. To this Hamiltonian should be applied trigonal symmetry breaking at all levels of interaction. All these ingredients are present in the microscopic Hamiltonian used to construct the expressions in Table 3. These expressions represent the most detailed model available for insight into ab initio results[31,42] and experimental magnetic[29,35] and spectral[43] data.

5. Exchange Interactions between Orbitally Degenerate Ions: The d^3–d^3 Case in Trigonal Symmetry

The chromium(III) dimer, $Cr_2X_9^{3-}$ (X = Cl^-, Br^-) presents us with a t_{2g}^3−t_{2g}^3 exchange problem, which highlights the role of multielectronic site configurations. In principle, the Hamiltonian formalism derived for $Ti_2X_9^{3-}$ can directly be applied to the $Cr_2X_9^{3-}$ case as well. However, highly untractable expressions result since there are already 400 covalent states and the transfer of one electron generates not less than 450 ionic states. We are thus forced to introduce some carefully chosen approximations, which are aimed at simplifying the denominators in the perturbation expansion. The zeroth-order Hamiltonian is thus divided in a barycenter part, H_0, which contains the average intra- and intersite Coulomb repulsion, and a remainder, H_0', which contains the multiplet fine structure. To these is added the usual transfer term, V

$$H = H_0 + H_0' + V \tag{37}$$

$$H_0 = U\Big(\sum_i (n_{i\alpha}^A n_{i\beta}^A + n_{i\alpha}^B n_{i\beta}^B) + \sum_{i<j}\sum_{\sigma\sigma'} (n_{i\sigma}^A n_{j\sigma'}^A + n_{i\sigma}^B n_{j\sigma'}^B)\Big) + U'\sum_{i,j}\sum_{\sigma\sigma'} n_{i\sigma}^A n_{j\sigma'}^B \tag{38}$$

$$H_0' = H_0'(A) + H_0'(B) + H_0'(AB)$$

$$H_0'(A) = (U_{\parallel} - U)\sum_i n_{i\alpha}^A n_{i\beta}^A + (U_{\perp} - U)\sum_{i<j,\sigma\sigma'} n_{i\sigma}^A n_{j\sigma'}^A - \frac{1}{2}J\sum_{i\neq j}\sum_{\sigma}(n_{i\sigma}^A n_{j\sigma}^A - a_{i\sigma}^\dagger a_{j\sigma} a_{i-\sigma}^\dagger a_{j-\sigma} - a_{i\sigma}^\dagger a_{j\sigma} a_{j-\sigma}^\dagger a_{i-\sigma}) + \Delta\sum_\sigma (n_{\theta\sigma}^A + n_{\epsilon\sigma}^A)$$

$$H_0'(AB) = \sum_{i,j}\sum_{\sigma\sigma'}(U_{ijij} - U')\, n_{i\sigma}^A n_{j\sigma'}^B + \sum_{i\neq j}\sum_{\sigma\sigma'} U_{iijj}(a_{i\sigma}^\dagger a_{j\sigma} b_{i\sigma'}^\dagger b_{j\sigma'} + a_{i\sigma}^\dagger a_{j\sigma} b_{j\sigma'}^\dagger b_{i\sigma'}) - \sum_i\sum_{\sigma\sigma'} B_{iiii}(a_{i\sigma}^\dagger a_{i\sigma'} b_{i\sigma'}^\dagger b_{i\sigma}) - \sum_{i\neq j}\sum_{\sigma\sigma'} B_{iijj} a_{i\sigma}^\dagger a_{j\sigma'} b_{i\sigma'}^\dagger b_{j\sigma} - \sum_{i\neq j}^{\sigma\sigma'} B_{ijji} a_{i\sigma}^\dagger a_{j\sigma'} b_{j\sigma'}^\dagger b_{j\sigma} - \sum_{i\neq j}\sum_{\sigma\sigma'} B_{ijij}(a_{i\sigma}^\dagger a_{j\sigma'} b_{i\sigma'}^\dagger b_{i\sigma}) \tag{39}$$

U and U' are, respectively, the average Coulomb repulsion between electrons on the same center and on different centers. The other parameters were already defined before. One has

$$U = \frac{U_{\parallel} + 4U_{\perp}}{5} \tag{40}$$

The pseudospherical relation for t_{2g} repulsion integrals, $2J = U_{\parallel} - U_{\perp}$, allows us to eliminate the $U_{\parallel}$ and $U_{\perp}$ parameters according to

$$U_{\parallel} - U = \frac{8}{5}J$$

$$U_{\perp} - U = -\frac{2}{5}J \tag{41}$$

The Hamiltonian which we have just described acts in a space of 924 states, comprising 400 covalent states with t_{2g}^3−t_{2g}^3 configuration, 450 monoexcited states with t_{2g}^4−t_{2g}^2 configuration, 72 biexcited states of t_{2g}^5−t_{2g}^1 type, and 2 triexcited t_{2g}^6−t_{2g}^0 states. As before, we now apply a projection operator S which acts in the space of H_0 eigenstates. Since H_0 no longer contains the multiplet fine structure, its eigenvalues, which appear as denominators in the projection operator, reduce to simple expressions for the average

repulsion in a given configuration. For a state $|\Phi_k^0\rangle$ belonging to $t_{2g}^{\bar{n}_A}-t_{2g}^{\bar{n}_B}$, one has

$$E_k = U\left[\frac{\bar{n}_A(\bar{n}_A-1)}{2}+\frac{\bar{n}_B(\bar{n}_B-1)}{2}\right]+U'\bar{n}_A\bar{n}_B \quad (42)$$

The remaining interactions, H_0' and V, are both treated as perturbations. The effective Hamiltonian thus becomes

$$\tilde{H} = H_0 + H_0' + [S, H_0'] + \frac{1}{2}[S, V] + \frac{1}{2}[S, [S, H_0']] + \frac{1}{2}[S, [S, V]] + \ldots \quad (43)$$

with

$$\frac{1}{2}[S, V] = \frac{1}{2}\sum_{kn}\left(\sum_l\left(\frac{1}{E_k-E_l}+\frac{1}{E_n-E_l}\right)V_{kl}\,V_{ln}\right)|\Phi_k^0\rangle\langle\Phi_n^0|$$

$$[S, H_0'] = \sum_{kls}\left(\frac{(H_0')_{lk}\,V_{sl}}{E_s-E_l}+\frac{(H_0')_{sl}\,V_{lk}}{E_k-E_l}\right)|\Phi_s^0\rangle\langle\Phi_k^0|$$

$$[S, [S, H_0']] = \sum_{np}\sum_{kl}\frac{V_{np}}{E_n-E_p}\left(\frac{(H_0')_{lk}\,V_{pl}}{E_p-E_l}+\frac{(H_0')_{pl}\,V_{lk}}{E_k-E_l}\right)\times (|\Phi_n^o\rangle\langle\Phi_k^0| + |\Phi_k^0\rangle\langle\Phi_n^0|)$$

$$[S, [S, V]] = \sum_{np}\sum_{kl}\frac{V_{np}\,V_{pl}\,V_{lk}}{E_n-E_p}\left(\frac{1}{E_p-E_l}+\frac{1}{E_k-E_l}\right)\times (|\Phi_n^o\rangle\langle\Phi_k^0| + |\Phi_k^0\rangle\langle\Phi_n^0|) \quad (44)$$

When working out the above expressions, we used the real Hermitian character of the matrices in V and H_0'. When the Hamiltonian acts on the ground manifold of covalent states, second-order transfer paths will only reach singly excited $t_{2g}^4-t_{2g}^2$ configurations at average energies $U - U'$. Under this restriction, the effective Hamiltonian reduces to

$$H_{eff} = H_0 + H_0' - \frac{1}{U-U'}V\cdot V - \frac{1}{2(U-U')^2}[[H_0', V], V] \quad (45)$$

The energies of the dimer coupled states appear when the effective Hamiltonian is confronted with the determinantal symmetry functions for the covalent manifold. The single-center $(t_{2g})^3$ wavefunctions[44] are listed in Table 5. The states are characterized by an orbital and spin label. The orbital component of the $^4A_{2g}$ ground state is denoted as a_0. The horizontal symmetry plane connects the two sites, e.g.

$$\hat{\sigma}_h|a_0(1/2)^A\rangle = |a_0(1/2)^B\rangle \quad (46)$$

Pair states are obtained by coupling single-center states with full antisymmetrization over all electrons, e.g.

$$|^7A_2''\rangle = \{a_0(3/2)^A\, a_0(3/2)^B\} = |a^A\,\theta^A\,\epsilon^A\,a^B\,\theta^B\,\epsilon^B| \quad (47)$$

Table 5. Single-Center Wave Functions for the $(t_{2g})^3$ Configuration[44]

$^4A_{2g}$	$a_0(3/2)$	=	$\lvert a\theta\epsilon\rvert$
	$a_0(1/2)$	=	$\frac{1}{\sqrt{3}}(\lvert a\theta\bar{\epsilon}\rvert + \lvert a\bar{\theta}\epsilon\rvert + \lvert\bar{a}\theta\epsilon\rvert)$
^2E_g	$\epsilon(1/2)$	=	$\frac{1}{\sqrt{6}}(\sqrt{2}\lvert a\bar{a}\theta\rvert - \sqrt{2}\lvert\theta\epsilon\bar{\epsilon}\rvert + \lvert a\theta\bar{\theta}\rvert - \lvert a\epsilon\bar{\epsilon}\rvert)$
	$\theta(1/2)$	=	$\frac{1}{\sqrt{6}}(\sqrt{2}\lvert a\bar{a}\epsilon\rvert - \sqrt{2}\lvert\theta\bar{\theta}\epsilon\rvert + \lvert a\bar{\theta}\epsilon\rvert - \lvert a\theta\bar{\epsilon}\rvert)$
$^2T_{1g}$	$a(1/2)$	=	$\frac{1}{\sqrt{6}}(2\lvert\bar{a}\theta\epsilon\rvert - \lvert a\bar{\theta}\epsilon\rvert - \lvert a\theta\bar{\epsilon}\rvert)$
	$\theta(1/2)$	=	$\frac{1}{\sqrt{6}}(-\sqrt{2}\lvert a\theta\bar{\theta}\rvert + \sqrt{2}\lvert a\epsilon\bar{\epsilon}\rvert - \lvert\theta\epsilon\bar{\epsilon}\rvert + \lvert a\bar{a}\theta\rvert)$
	$\epsilon(1/2)$	=	$\frac{1}{\sqrt{6}}(\sqrt{2}\lvert a\theta\bar{\epsilon}\rvert - \sqrt{2}\lvert a\bar{\theta}\epsilon\rvert + \lvert a\bar{a}\epsilon\rvert - \lvert\theta\bar{\theta}\epsilon\rvert)$

Relevant pair states in the low-energy region are the $^4A_{2g}-^4A_{2g}$ ground state combinations and the $^4A_{2g}-^2E_2$ and $^4A_{2g}-^2T_{1g}$ pairs involving excitations of a single site. These states are listed in Table 6.

Energy expressions[45] for all these states are given in Tables 7−9. The derivation of these expressions is a task of considerable complexity, which can only be carried out with the help of a symbol manipulating package such as Mathematica. For completeness, we also list the nonzero off-diagonal matrix elements in Table 10. Since the manifolds concerned are separated by approximately 15 000 cm^{-1}, these matrix elements are not used in our discussion.

A CASSCF calculation was performed on the lowest dimer states of $Cr_2Cl_9^{3-}$. The results and details of the calculation are indicated in Table 11. We will now summarize the main results from a comparison of model expressions, ab initio calculations, and spectral data.

We first consider the $^4A_{2g}-^4A_{2g}$ ground state. From the energy expressions in Table 7, it is obvious that the spin states which result from the coupling of the two $^4A_{2g}$ states obey a Landé-type interval rule. This means that we can describe the exchange interaction by a Heisenberg Hamiltonian of the type $H = -2J_{ex}\boldsymbol{S}_A\cdot\boldsymbol{S}_B$. The coupling constant J_{ex} has three ingredients which are defined in the table.

$$J_{ex} = J_f + 2J_a^{(1)} + 2J_a^{(2)} \quad (48)$$

$J_a^{(1)}$ is the kinetic part which is responsible for the antiferromagnetic ground state. As compared to the ground state of $Ti_2Cl_9^{3-}$, the principal $t_a^2/(U-U')$ contribution in $J_a^{(1)}$ is reduced by a statistical factor of 1/9. As a result, the other contributions, the ferromagnetic term, J_f, and the repulsion-assisted exchange, $J_a^{(2)}$, gain importance. Both terms reduce the antiferromagnetic gap. J_{ex} can be estimated using the parameter values that were previously[31] obtained

Table 6. Determinant Functions for the Excited States of the $(t_{2g})^3-(t_{2g})^3$ Configuration[a]

$^4A_{2g} \times {}^4A_{2g}$	$^7A_2''$	=	$a_0(3/2)^A a_0(3/2)^B)$
	$^5A_1'$	=	$\frac{1}{\sqrt{2}}(a_0(3/2)^A a_0(1/2)^B - a_0(1/2)^A a_0(3/2)^B)$
	$^3A_2''$	=	$\frac{1}{\sqrt{10}}(\sqrt{3}a_0(3/2)^A a_0(-1/2)^B - 2a_0(1/2)^A a_0(1/2)^B + \sqrt{3}a_0(-1/2)^A a_0(3/2)^B)$
	$^1A_1'$	=	$\frac{1}{2}(-a_0(1/2)^A a_0(-1/2)^B + a_0(-1/2)^A a_0(1/2)^B + a_0(3/2)^A a_0(-3/2)^B - a_0(-3/2)^A a_0(3/2)^B)$
$^4A_{2g} \times {}^2E_g$	$^5E'$	=	$\frac{1}{\sqrt{2}}(a_0(3/2)^A \theta(1/2)^B - \theta(1/2)^A a_0(3/2)^B)$
	$^3E'$	=	$\frac{1}{2\sqrt{2}}(-a_0(1/2)^A \theta(1/2)^B + \sqrt{3}a_0(3/2)^A \theta(-1/2)^B + \theta(1/2)^A a_0(1/2)^B - \sqrt{3}\theta(-1/2)^A a_0(3/2)^B)$
	$^5E''$	=	$\frac{1}{\sqrt{2}}(a_0(3/2)^A \theta(1/2)^B + \theta(1/2)^A a_0(3/2)^B)$
	$^3E''$	=	$\frac{1}{2\sqrt{2}}(-a_0(1/2)^A \theta(1/2)^B + \sqrt{3}a_0(3/2)^A \theta(-1/2)^B - \theta(1/2)^A a_0(1/2)^B + \sqrt{3}\theta(-1/2)^A a_0(3/2)^B)$
$^4A_{2g} \times {}^2T_{1g}$	$^5A_2''$	=	$\frac{1}{\sqrt{2}}(a_0(3/2)^A a(1/2)^B + a(1/2)^A a_0(3/2)^A)$
	$^3A_2''$	=	$\frac{1}{2\sqrt{2}}(-a_0(1/2)^A a(1/2)^B + \sqrt{3}a_0(3/2)^A a(-1/2)^B - a(1/2)^A a_0(1/2)^B + \sqrt{3}a(-1/2)^A a_0(3/2)^B)$
	$^5A_1'$	=	$\frac{1}{\sqrt{2}}(a_0(3/2)^A a(1/2)^B - a(1/2)^A a_0(3/2)^B)$
	$^3A_1'$	=	$\frac{1}{2\sqrt{2}}(-a_0(1/2)^A a(1/2)^B + \sqrt{3}a_0(3/2)^A a(-1/2)^B + a(1/2)^A a_0(1/2)^B - \sqrt{3}a(-1/2)^A a_0(3/2)^B)$
	$^5E'$	=	$\frac{1}{\sqrt{2}}(a_0(3/2)^A \theta(1/2)^B - \theta(1/2)^A a_0(3/2)^B)$
	$^3E'$	=	$\frac{1}{2\sqrt{2}}(-a_0(1/2)^A \theta(1/2)^B + \sqrt{3}a_0(3/2)^A \theta(-1/2)^B + \theta(1/2)^A a_0(1/2)^B - \sqrt{3}\theta(-1/2)^A a_0(3/2)^B)$
	$^5E''$	=	$\frac{1}{\sqrt{2}}(a_0(3/2)^A \theta(1/2)^B + \theta(1/2)^A a_0(3/2)^B)$
	$^3E''$	=	$\frac{1}{2\sqrt{2}}(-a_0(1/2)^A \theta(1/2)^B + \sqrt{3}a_0(3/2)^A \theta(-1/2)^B - \theta(1/2)^A a_0(1/2)^B + \sqrt{3}\theta(-1/2)^A a_0(3/2)^B)$

[a] For the E-type functions, only the θ component is given.

for $Ti_2Cl_9^{3-}$ with a similar metal−metal distance. This yields a value of -20 cm^{-1}, which is less antiferromagnetic than could be expected from the statistical factor alone.

The model thus leads to two important predictions: (*i*) the splitting between the spin states of the ground configurations should follow a Landé interval rule, and (*ii*) the coupling is antiferromagnetic with a singlet−triplet gap in $Cr_2Cl_9^{3-}$ of approximately 40 cm^{-1}, which is far less than 1/9 of the 800 cm^{-1} gap in the comparable $t_{2g}{}^1-t_{2g}{}^1$ Ti(III) system. These predictions now have to be compared with experimental and ab initio results.

The ab initio results for $Cr_2Cl_9^{3-}$ were listed in Table 11. A broad spectrum of experimental splittings is collected in Table 12.

These data were obtained from magnetic susceptibility,[46] optical,[47] high-resolution Zeeman and MCD,[47,48] INS,[49] and ESR[50,51] measurements. In addition, a wealth of experimental information is also available on similar triply bridged complexes

Table 7. Parametric Energy Expressions for $^4A_{2g}-{}^4A_{2g}$

state	energy[a]
$^7A_2''$	$h_g - 9J_f$
$^5A_1'$	$h_g - 3J_f + 12J_a^{(1)} + 12J_a^{(2)}$
$^3A_2''$	$h_g + J_f + 20J_a^{(1)} + 20J_a^{(2)}$
$^1A_1'$	$h_g + 3J_f + 24J_a^{(1)} + 24J_a^{(2)}$

[a] $h_g = 6U - (42/5)J + 4\Delta + U_{aaaa} + 2(U_{\theta\theta\theta\theta} + U_{\theta\epsilon\theta\epsilon}) + 4U_{a\theta a\theta}$. $J_f = (1/9)(B_{aaaa} + 4B_{a\theta\theta a} + 2(B_{\theta\theta\theta\theta} + B_{\theta\theta\epsilon\epsilon}))$ $J_a^{(1)} = -(1/9(U - U'))(t_a^2 + 2t_e^2)$ $J_a^{(2)} = (1/9(U - U')^2)(t_a^2(18/5\ J + U' - U_{aaaa}) - 4t_at_eU_{aa\theta\theta} + 2t_e^2(18/5\ J + U' - U_{\theta\theta\theta\theta} - U_{\theta\theta\epsilon\epsilon}))$.

such as $Cr_2Br_9^{3-}$ [52–54] and tris-μ-hydroxo Cr(III) complexes with Wieghardt-type ligands.[55–60]

The derivations of the Landé interval rule can be expressed by adding higher order terms to the phenomenological Hamiltonian

$$H_{ex} = -2J_{ex}\boldsymbol{S}_A\cdot\boldsymbol{S}_B + j(\boldsymbol{S}_A\cdot\boldsymbol{S}_B)^2 + \Delta_3(\boldsymbol{S}_A\cdot\boldsymbol{S}_B)^3 \qquad (49)$$

In Table 13 we summarize the values for the three parameters J_{ex}, j, and Δ_3 that can be extracted from experiment.

The experimental data which we have retrieved do not provide convincing evidence for significant deviations from the Landé rule. In fact, the only experiment which supports such deviation is the ESR study of $(NPr_4)_3Cr_2Cl_9$.[51] The reason for this discrepancy is unclear. The ab initio calculations on $Cr_2Cl_9^{3-}$ also exhibit a negative deviation from the interval rule. The size of the calculated singlet−triplet gap at the CASPT2(c) level is almost in quantitative agreement with our extrapolated value from $Ti_2Cl_9^{3-}$ but clearly overestimates the true gap. One possible explanation would be that in spite of the similar metal−metal distance the hopping integral for through-space $d_{z^2}-d_{z^2}$ overlap in $Cr_2Cl_9^{3-}$ is much smaller than in $Ti_2Cl_9^{3-}$, as suggested by Güdel and Leuenberger on the basis of extended Hückel calculations.[61]

Next we turn our attention to the excited states of $^4A_{2g}-{}^2E_g$ and $^4A_{2g}-{}^2T_{1g}$ parentage.

These excited pair states have formed the object of experimental[46–48,52] and theoretical[62,63] studies. One conclusion, on which there seems to be at least general agreement, is that the exchange interaction in these excited manifolds is a very complicated problem, which remains poorly understood. Ligand-field absorption spectra of $Cs_3Cr_2Cl_9$ and $Cs_3Cr_2Br_9$ have been obtained by Dubicki et al.[52] For the bromide complex the spin-paired $t_{2g}{}^3-t_{2g}{}^3$ states are clearly observable in the optical windows between the intense spin-allowed $t_{2g} \rightarrow e_g$ bands. For the chloride complex only the $^4A_{2g}-{}^2T_{1g}$ region could well be characterized by polarized absorption spectroscopy.[48] One of the most interesting model treatments was presented by Barry et al. in 1981.[63] Using little more than symmetry and spin operators, these authors arrived at a valuable result regarding the energy difference between prime and double prime states of a given spin. The ratio of these differences in the quintet vs the triplet states was found to adopt the simple integer value of −3. Hence, as an example, for the energies of the E-states originating from the $^4A_{2g}-{}^2E_g$ manifold one would have

$$\frac{{}^5E' - {}^5E''}{{}^3E' - {}^3E''} = -3 \qquad (50)$$

Table 8. Parametric Energy Expressions for $^4A_{2g}-{}^2E_g$

state	energy[a]
$^5E''$	$h_{ae} + \frac{1}{3}(-2B_{aaaa} - 2B_{aa\theta\theta} - 8B_{a\theta\theta a} - 2B_{a\theta a\theta} - 5B_{\theta\theta\theta\theta} - 3B_{\epsilon\theta\theta\epsilon})$ $+\frac{1}{3(U-U')}(-2t_a^2 - 2t_e^2 + 4t_at_e)$ $+\frac{1}{3(U-U')^2}[t_a^2(\frac{6}{5}J + 2U' + 2U_{aa\theta\theta} - 2U_{a\theta a\theta})$ $+ t_e^2(\frac{6}{5}J + 2U' + 2U_{aa\theta\theta} - 2U_{a\theta a\theta})$ $+ t_at_e(\frac{-12}{5}J - 4U' - 4U_{aa\theta\theta} + 4U_{a\theta a\theta})]$
$^3E''$	$h_{ae} + \frac{1}{9}(-2B_{aaaa} + 2B_{aa\theta\theta} - 8B_{a\theta\theta a} + 2B_{a\theta a\theta} - 3B_{\theta\theta\theta\theta} - 5B_{\theta\epsilon\epsilon\theta})$ $+\frac{1}{9(U-U')}(-14t_a^2 - 30t_e^2 - 4t_at_e)$ $+\frac{1}{9(U-U')^2}[t_a^2(\frac{162}{5}J + 14U' - 8U_{aaaa} - 2U_{aa\theta\theta} - 6U_{a\theta a\theta})$ $+ t_e^2(\frac{330}{5}J + 30U' - 2U_{aa\theta\theta} - 6U_{a\theta a\theta} - 24U_{\theta\theta\theta\theta} - 8U_{\theta\theta\epsilon\epsilon})$ $+ t_at_e(\frac{12}{5}J + 4U' - 44U_{aa\theta\theta} - 4U_{a\theta a\theta})]$
$^3E'$	$h_{ae} + \frac{1}{9}(-2B_{aaaa} - 2B_{aa\theta\theta} - 8B_{a\theta\theta a} - 2B_{a\theta a\theta} - 5B_{\theta\theta\theta\theta} - 3B_{\theta\epsilon\epsilon\theta})$ $+\frac{1}{9(U-U')}(-14t_a^2 - 26t_e^2 + 4t_at_e)$ $+\frac{1}{9(U-U')^2}[t_a^2(\frac{162}{5}J + 14U' - 8U_{aaaa} + 2U_{aa\theta\theta} - 6U_{a\theta a\theta})$ $+ t_e^2(\frac{318}{5}J + 26U' + 2U_{aa\theta\theta} - 6U_{a\theta a\theta} - 20U_{\theta\theta\theta\theta} - 12U_{\theta\theta\epsilon\epsilon})$ $+ t_at_e(\frac{-12}{5}J - 4U' - 44U_{aa\theta\theta} + 4U_{a\theta a\theta})]$
$^5E'$	$h_{ae} + \frac{1}{3}(-2B_{aaaa} + 2B_{aa\theta\theta} - 8B_{a\theta\theta a} + 2B_{a\theta a\theta} - 3B_{\theta\theta\theta\theta} - 5B_{\theta\epsilon\epsilon\theta})$ $+\frac{1}{3(U-U')}(-2t_a^2 - 6t_e^2 - 4t_at_e)$ $+\frac{1}{3(U-U')^2}[t_a^2(\frac{6}{5}J + 2U' - 2U_{aa\theta\theta} - 2U_{a\theta a\theta})$ $+ t_e^2(\frac{18}{5}J + 6U' - 2U_{aa\theta\theta} - 2U_{a\theta a\theta} - 4U_{\theta\theta\theta\theta} + 4U_{\theta\theta\epsilon\epsilon})$ $+ t_at_e(\frac{12}{5}J + 4U' - 4U_{aa\theta\theta} - 4U_{a\theta a\theta})]$

[a] $h_{ae} = 6U - (27/5)J + 4\Delta + U_{aaaa} + 2(U_{\theta\theta\theta\theta} + U_{\theta\epsilon\theta\epsilon}) + 4U_{a\theta a\theta}$.

Table 9. Parametric Energy Expressions for $^4A_{2g}-{}^2T_{1g}$

state	energy[a]
$^5A_2''$	$h_{at} - B_{aaaa} - B_{a\theta\theta a} - 2B_{\theta\theta\theta\theta} - 2B_{\theta\epsilon\epsilon\theta}$
$^5A_1'$	$h_{at} + \frac{1}{3}(B_{aaaa} - 11B_{a\theta\theta a} - 4B_{\theta\theta\theta\theta} - 4B_{\theta\epsilon\epsilon\theta})$ $+\frac{1}{3(U-U')}(-8t_a^2 - 4t_e^2)$ $+\frac{1}{3(U-U')^2}[t_a^2(\frac{24}{5}J + 8U' - 8U_{aaaa})$ $+ t_e^2(\frac{12}{5}J + 4U' - 4U_{\theta\theta\theta\theta} - 4U_{\theta\theta\epsilon\epsilon})$ $+ 16t_at_eU_{aa\theta\theta}]$
$^3A_2''$	$h_{at} + \frac{1}{9}(-5B_{aaaa} - 17B_{a\theta\theta a} + 2B_{\theta\theta\theta\theta} + 2B_{\theta\epsilon\epsilon\theta})$ $+\frac{1}{9(U-U')}(-8t_a^2 - 40t_e^2)$ $+\frac{1}{9(U-U')^2}[t_a^2(\frac{24}{5}J + 8U' - 8U_{aaaa})$ $+ t_e^2(\frac{480}{5}J + 40U' - 40U_{\theta\theta\theta\theta} - 40U_{\theta\theta\epsilon\epsilon})$ $+ 16t_at_eU_{aa\theta\theta}]$
$^3A_1'$	$h_{at} - B_{aaaa} - B_{a\theta\theta a}$ $+\frac{1}{(U-U')}(-4t_e^2)$ $+\frac{1}{9(U-U')^2}t_e^2(\frac{468}{5}J + 36U' - 36U_{\theta\theta\theta\theta} - 36U_{\theta\theta\epsilon\epsilon})$
$^3E'$	$h_{at} + \frac{1}{18}(B_{aaaa} - 2B_{aa\theta\theta} - -11B_{a\theta\theta a} - 2B_{a\theta a\theta} - 13B_{\theta\theta\theta\theta} - 4B_{\theta\theta\epsilon\epsilon} - 13B_{\theta\epsilon\epsilon\theta} - 4B_{\theta\epsilon\theta\epsilon})$ $+\frac{1}{9(U-U')}(-19t_a^2 - 19t_e^2 + 2t_at_e)$ $+\frac{1}{9(U-U')^2}[t_a^2(\frac{237}{5}J + 19U' - 16U_{aaaa} + U_{aa\theta\theta} - 3U_{a\theta a\theta})$ $+ t_e^2(\frac{237}{5}J + 19U' + U_{aa\theta\theta} - 3U_{a\theta a\theta} - 8U_{\theta\theta\theta\theta} - 16U_{\theta\theta\epsilon\epsilon} - 8U_{\theta\epsilon\theta\epsilon})$ $+ t_at_e(\frac{-6}{5}J - 2U' - 46U_{aa\theta\theta} + 2U_{a\theta a\theta})]$
$^3E''$	$h_{at} + \frac{1}{18}(B_{aaaa} + 2B_{aa\theta\theta} - 11B_{a\theta\theta a} + 2B_{a\theta a\theta} - 13B_{\theta\theta\theta\theta} + 4B_{\theta\theta\epsilon\epsilon} - 13B_{\theta\epsilon\epsilon\theta} + 4B_{\theta\epsilon\theta\epsilon})$ $+\frac{1}{9(U-U')}(-19t_a^2 - 27t_e^2 - 2t_at_e)$ $+\frac{1}{9(U-U')^2}[t_a^2(\frac{237}{5}J + 19U' - 16U_{aaaa} - U_{aa\theta\theta} - 3U_{a\theta a\theta})$ $+ t_e^2(\frac{261}{5}J + 27U' - U_{aa\theta\theta} - 3U_{a\theta a\theta} - 8U_{\theta\theta\theta\theta} - 24U_{\theta\theta\epsilon\epsilon} - 16U_{\theta\epsilon\theta\epsilon})$ $+ t_at_e(\frac{6}{5}J + 2U' - 46U_{aa\theta\theta} - 2U_{a\theta a\theta})]$
$^5E''$	$h_{at} + \frac{1}{6}(-5B_{aaaa} - 2B_{aa\theta\theta} - 17B_{a\theta\theta a} - 2B_{a\theta a\theta} - 7B_{\theta\theta\theta\theta} - 4B_{\theta\theta\epsilon\epsilon} - 7B_{\theta\epsilon\epsilon\theta} - 4B_{\theta\epsilon\theta\epsilon})$ $+\frac{1}{3(U-U')}(-t_a^2 - t_e^2 + 2t_at_e)$ $+\frac{1}{3(U-U')^2}[t_a^2(\frac{3}{5}J + U' + U_{aa\theta\theta} - U_{a\theta a\theta})$ $+ t_e^2(\frac{3}{5}J + U' + U_{aa\theta\theta} - U_{a\theta a\theta})$ $+ t_at_e(\frac{-6}{5}J - 2U' - 2U_{aa\theta\theta} + 2U_{a\theta a\theta})]$
$^5E'$	$h_{at} + \frac{1}{6}(-5B_{aaaa} + 2B_{aa\theta\theta} - 17B_{a\theta\theta a} + 2B_{a\theta a\theta} - 7B_{\theta\theta\theta\theta} + 4B_{\theta\theta\epsilon\epsilon} - 7B_{\theta\epsilon\epsilon\theta} + 4B_{\theta\epsilon\theta\epsilon})$ $+\frac{1}{3(U-U')}(-t_a^2 - 9t_e^2 - 2t_at_e)$ $+\frac{1}{3(U-U')^2}[t_a^2(\frac{3}{5}J + U' - U_{aa\theta\theta} - U_{a\theta a\theta})$ $+ t_e^2(\frac{27}{5}J + 9U' - U_{aa\theta\theta} - U_{a\theta a\theta} - 8U_{\theta\theta\epsilon\epsilon} - 8U_{\theta\epsilon\theta\epsilon})$ $+ t_at_e(\frac{6}{5}J + 2U' - 2U_{aa\theta\theta} - 2U_{a\theta a\theta})]$

[a] $h_{at} = 6U - (27/5)J + 4\Delta + U_{aaaa} + 2(U_{\theta\theta\theta\theta} + U_{\theta\epsilon\theta\epsilon}) + 4U_{a\theta a\theta}$.

Table 10. Off-diagonal Exchange Matrix Elements between the $^4A_{2g}-{}^4A_{2g}$ and $^4A_{2g}-{}^2T_{1g}$ Configurations

$\langle {}^5A_1'({}^4A_{2g}\,{}^4A_{2g})\lvert H_{eff}\rvert {}^5A_1'({}^4A_{2g}\,{}^2T_{1g})\rangle$	$\frac{2\sqrt{2}}{3}(B_{aaaa} + B_{a\theta\theta a} - B_{\theta\theta\theta\theta} - B_{\theta\epsilon\epsilon\theta})$ $+\frac{4\sqrt{2}}{3(U-U')}(-t_a^2 + t_e^2)$ $+\frac{\sqrt{2}}{3(U-U')^2}[t_a^2(\frac{42}{5}J + 4U' - 4U_{aaaa})$ $+ t_e^2(-\frac{42}{5}J - 4U' + 4U_{\theta\theta\theta\theta} + 4U_{\theta\theta\epsilon\epsilon})$ $- 4t_at_eU_{aa\theta\theta}]$
$\langle {}^3A_2''({}^4A_{2g}\,{}^4A_{2g})\lvert H_{eff}\rvert {}^3A_2''({}^4A_{2g}\,{}^2T_{1g})\rangle$	$\frac{4+6\sqrt{2}}{9\sqrt{5}}(B_{aaaa} + B_{a\theta\theta a} - B_{\theta\theta\theta\theta} - B_{\theta\epsilon\epsilon\theta})$ $+\frac{-8+12\sqrt{2}}{9\sqrt{5}(U-U')}(-t_a^2 + t_e^2)$ $+\frac{2+3\sqrt{2}}{9\sqrt{5}(U-U')^2}[t_a^2(\frac{42}{5}J + 4U' - 4U_{aaaa})$ $+ t_e^2(-\frac{42}{5}J - 4U' + 4U_{\theta\theta\theta\theta} + 4U_{\theta\theta\epsilon\epsilon})$ $- 4t_at_eU_{aa\theta\theta}]$

This result was based on explicit calculation of a few two-electron matrix elements.

Quite remarkably the result obtained by Barry et al.[63] also applies to the full energy expressions in Tables 8 and 9, which are based on a much more elaborate Hamiltonian and comprise all possible two-body interactions. Undoubtedly this relationship is due to the aufbau symmetry of the half-filled shell states, which also underlies the quasispin selection rules in the doublet states of monomeric Cr(III) complexes.[64] From this symmetry we can build a two-parameter spin Hamiltonian, which presents a unified treatment of the pair states

$$H = J_1 \boldsymbol{S}_A \cdot \boldsymbol{S}_B + J_2(-1)^S \boldsymbol{S}^2 \hat{\sigma}_h \qquad (51)$$

Table 11. Calculated Energy Spectrum[a] of $Cr_2Cl_9^{3-}$

		CASSCF	CASPT2(v)	CASPT2(c)
$^4A_{2g}$ $^4A_{2g}$	$^1A_1'$	0	0	0
	$^3A_2''$	4	41	44
	$^5A_1'$	10	104	112
	$^7A_2''$	18	150	163
$^4A_{2g}$ ^2E_g	$^5E''$	19166	16700	14600
	$^3E''$	19182	16703	14599
	$^3E'$	19175	16714	14617
	$^5E'$	19186	16731	14627
$^4A_{2g}$ $^2T_{1g}$	$^5A_1'$	19787	17245	15335
	$^3A_2''$	19830	17423	15526
	$^5A_2''$	19839	17473	15581
	$^3A_1'$	19847	17494	15604
	$^3E'$	20262	17631	15607
	$^3E''$	20264	17638	15614
	$^5E''$	20280	17759	15743
	$^5E'$	20288	17776	15763

[a] Basis set used 6s4p3d1f on Cr, 4s3p1d on Cl.

Table 12. Experimental Energy Splittings (in cm^{-1}) for the Ground State of $Cr_2Cl_9^{3-}$

	ref	$^7A_2''-{}^5A_1'$	$^5A_1'-{}^3A_2''$	$^3A_2''-{}^1A_1'$
$Cr_2Cl_9^{3-}$	51	23 ± 2.5	27 ± 1.5	11 ± 0.5
	47	39 ± 0.5	26 ± 0.5	13 ± 0.5
	48	39 ± 4	26 ± 1	12 ± 1
	49			14.1
$Cr_2Br_9^{3-}$	52	13	10.5	8.5
	54			8.3
$Cr_2(OH)_3(tmtacn)_2$	57	not measured	267 ± 1.5	138 ± 0.5
	58	not measured	211 ± 7	112 ± 2

Table 13. Experimental Values for the Ground-State Exchange Parameters for the Hamiltonian in eq 49

	ref	J	j	Δ_3
$Cr_2Cl_9^{3-}$	50	−5.9		
	46	−6.5	≈0	
	51	−6.2	−1.75	−0.34
	47	−6.2	$0 \geq j \geq -0.5$	
	48	−6.7	0.25	
$Cr_2Br_9^{3-}$	52	−4.2	−0.2	
$Cr_2(OH)_3(tmtacn)_2$	57	−64	−1.6	
	58	−51	−1.2	

where J_1 and J_2 are two exchange parameters, $\boldsymbol{S}^2$ is the total spin momentum operator, and $\hat{\sigma}_h$ recognizes the spatial symmetry of the orbital part. The four states $^3\Gamma'$, $^3\Gamma''$, $^5\Gamma'$,$^5\Gamma''$ of a given manifold ($\Gamma = E$ for $^4A_{2g}-{}^2E_g$, $\Gamma = A$, E for $^4A_{2g}-{}^2T_{1g}$) are split by this Hamiltonian as follows

$$\begin{aligned} E(^5\Gamma') &= 3/4J_1 + 6J_2 \\ E(^5\Gamma'') &= 3/4J_1 - 6J_2 \\ E(^3\Gamma') &= -5/4J_1 - 2J_2 \\ E(^3\Gamma'') &= -5/4J_1 + 2J_2 \end{aligned} \tag{52}$$

In this parametrization scheme the energy gap between $^5\Gamma'$ and $^5\Gamma''$ equals $12J_2$, versus $-4J_2$ for the triplet levels, yielding the required ratio of −3. The separation between the quintet and triplet barycenters amounts to $2J_1$.

We will now discuss in detail the $^4A_{2g}-{}^2E_g$ states. From Table 8 we can deduce the expressions for the J_1 and J_2 parameters:

$$\begin{aligned} J_1 = \frac{1}{9}\Bigg[&-2B_{aaaa} - 8B_{a\theta\theta a} - 4B_{\theta\theta\theta\theta} - 4B_{\theta\epsilon\epsilon\theta} + \\ &\frac{1}{U-U'}(4t_a^2 + 8t_e^2) + \frac{1}{(U-U')^2} \times \\ &\left(t_a^2\left(\frac{-72}{5}J - 4U' + 4U_{aaaa}\right) + t_a t_e 16U_{aa\theta\theta} + \right. \\ &\left. t_e^2\left(\frac{-288}{5}J - 8U' + 8U_{\theta\theta\theta\theta} + 8U_{\theta\theta\epsilon\epsilon}\right)\right)\Bigg] \end{aligned} \tag{53}$$

$$\begin{aligned} J_2 = \frac{1}{18}\Bigg[&2B_{aa\theta\theta} + 2B_{a\theta a\theta} + B_{\theta\theta\theta\theta} - B_{\theta\epsilon\epsilon\theta} + \\ &\frac{1}{U-U'}(-2t_e^2 - 4t_a t_e) + \frac{1}{(U-U')^2} \times \\ &\left(t_a^2(-2U_{aa\theta\theta}) + t_a t_e\left(\frac{12}{5}J + 4U' - 4U_{a\theta a\theta}\right) + \right. \\ &\left. t_e^2\left(\frac{6}{5}J + 2U' - 2U_{aa\theta\theta} - 2U_{\theta\theta\theta\theta} + 2U_{\theta\theta\epsilon\epsilon}\right)\right)\Bigg] \end{aligned}$$

For the purpose of a semiqualitative analysis, we now make the following assumptions: (*i*) all B parameters are of the same order of magnitude, we summarize all these contributions into an effective B' parameter; (*ii*) since $t_a/t_e \approx -7$, t_e^2 can be neglected with respect to $t_a t_e$ and $t_a t_e$ can be neglected with respect to t_a^2.

The expressions for J_1 and J_2 within the $^4A_{2g}-{}^2E_g$ manifold are then written

$$\begin{aligned} J_1 &= \frac{1}{9}\left[-18B' + \frac{1}{U-U'}4t_a^2 + \frac{1}{(U-U')^2}t_a^2\left(\frac{-72}{5}J - 4U' + 4U_{aaaa}\right)\right] \\ J_2 &= \frac{1}{9}\left[2B' - \frac{1}{U-U'}2t_a t_e - \frac{1}{(U-U')^2}t_a^2\, U_{aa\theta\theta}\right] \end{aligned} \tag{54}$$

As can be seen above, J_1 should be a small parameter, because of the different contributions of opposite sign, and thus, the coupling can be ferro- or antiferromagnetic. J_2 should be larger, because now the leading terms both make a positive contribution, and thus, our calculation predicts that the prime quintet states will be higher in energy than the double prime quintet states. In Table 14 are the experimental energies for the $^4A_{2g}-{}^2E_g$ states in $Cr_2Br_9^{3-}$ as obtained by Dubicki et al.[52] The ordering here is ferromagnetic, but the quintet−triplet gap is very small (∼6 cm^{-1}). The splitting between prime and double prime states is much larger, 70 cm^{-1} for

Table 14. Spectroscopic Results for the Ordering of Pair States in $Cr_2X_9^{3-}$

	ref	state	energy
$^4A_{2g}-^2E_g$ $Cr_2Br_9^{3-}$	52	$^5E''$	13825
		$^3E'$	13856
		$^3E''$	13876
		$^5E'$	13895
$^4A_{2g}-^2T_{1g}$ $Cr_2Br_9^{3-}$	48	$^5A_1'$	14327
		$^5A_2''$	14486
		$^3A_2''$	14514
		$^3A_1'$	14554
		$^3E'$	14586
		$^3E''$	14600
		$^5E''$	not assigned
		$^5E'$	not assigned

the quintets and 20 cm^{-1} for the triplets. The experimental ratio amounts to

$$\frac{^5E' - ^5E''}{^3E' - ^3E''} \approx -3.5,$$

which is in good agreement with our calculations. For the $Cr_2Cl_9^{3-}$ complex, we have to rely upon the ab initio results in Table 11. On all levels of calculation, the coupling is ferromagnetic and smaller than the prime−double prime gap. At the CASSCF level, the ratio $(^5E' - ^5E'')/(^3E' - ^3E'')$ almost exactly equals the magic −3 ratio, an astonishing result which disappears upon introducing more correlation. Recently, Schenker et al.[65] found evidence for an antiferromagnetic coupling in the $^4A_{2g}-^2E_g$ manifold in tris(μ-hydroxo)bis(tmtame)chromium trinitrate (tmtame = *N*,*N*′,*N*″-trimethyl-1,1,1-tris(aminomethyl)ethane), but further information regarding the position of the quintet states could not be deduced. In the Wieghardt complex, tris(μ-hydroxo)bis(tmtacn)chromium triperchlorate (tmtacn = 1,4,7-trimethyl-1,4,7-triazacyclononane), Riesen et al.[57] also observed an antiferromagnetic coupling, but again, further information on the quintets was lacking. Since the kinetic part of the exchange in these complexes is much larger, J_1 will clearly be large and positive, which simply explains this observation. In both examples the $^3E''$ and $^3E'$ states are quite close to each other. The $^3E''$ is placed lowest as opposed to the $Cr_2X_9^{3-}$ complexes.[66] Riesen and Güdel point out that the t_{2g}^3 multiplets in the trial complexes are heavily mixed by the trigonal field, which may explain the different behavior of the lowest excited states.

Finally, let us consider the $^4A_{2g}-^2T_{1g}$ states. The trigonal field splits the parent $^2T_{1g}$ state into *A* and *E* components. Because of quasispin selection rules,[64] this is a second-order process involving ligand-field interaction between $^2T_{1g}$ and $^2T_{2g}$. The calculations for $Cr_2Cl_9^{3-}$ place the A states a few hundred cm^{-1} below the E states, and this is also confirmed experimentally.[48] For this reason the $\Gamma = A$ and $\Gamma = E$ manifolds can be treated separately as far as the exchange coupling is concerned. Again, for these cases the ratio of −3 is confirmed both at the CASSCF level and for the microscopic energy expressions as provided in Table 9. The experimental splittings are give in Table 14.

The J_1 and J_2 parameters are now expressed as follows. For the *A* manifold:

$$J_1 = \frac{1}{9}\Big[2B_{aaaa} - 4B_{a\theta\theta a} - 8B_{\theta\theta\theta\theta} - 8B_{\theta\epsilon\epsilon\theta} + \frac{1}{U-U'}(-4t_a^2 + 16t_e^2) + \frac{1}{(U-U')^2}\times \Big(t_a^2\Big(\frac{12}{5}J + 4U' - 4U_{aaaa}\Big) + 8t_at_eU_{aa\theta\theta} + t_e^2\Big(\frac{-228}{5}J - 16U' + 16U_{\theta\theta\theta\theta} + 16U_{\theta\theta\epsilon\epsilon}\Big)\Big)\Big]$$

$$J_2 = \frac{1}{18}\Big[2B_{aaaa} - 4B_{a\theta\theta a} + B_{\theta\theta\theta\theta} + B_{\theta\epsilon\epsilon\theta} + \frac{1}{U-U'}(-4t_a^2 - 2t_e^2) + \frac{1}{(U-U')^2}\times \Big(t_a^2\Big(\frac{12}{5}J + 4U' - 4U_{aaaa}\Big) + 8t_at_eU_{aa\theta\theta} + t_e^2\Big(\frac{6}{5}J + 2U' - 2U_{\theta\theta\theta\theta} - 2U_{\theta\theta\epsilon\epsilon}\Big)\Big)\Big] \quad (55)$$

And for the *E* manifold:

$$J_1 = \frac{1}{9}\Big[-4B_{aaaa} - 10B_{a\theta\theta a} - 2B_{\theta\theta\theta\theta} - 2B_{\theta\epsilon\epsilon\theta} + \frac{1}{U-U'}(8t_a^2 + 4t_e^2) + \frac{1}{(U-U')^2}\times \Big(t_a^2\Big(\frac{-114}{5}J - 8U' + 8U_{aaaa}\Big) + 20t_at_eU_{aa\theta\theta} + t_e^2\Big(\frac{-102}{5}J - 4U' + 4U_{\theta\theta\theta\theta} + 4U_{\theta\theta\epsilon\epsilon}\Big)\Big)\Big]$$

$$J_2 = \frac{1}{18}\Big[B_{aa\theta\theta} + B_{a\theta a\theta} + 2B_{\theta\theta\epsilon\epsilon} + 2B_{\theta\epsilon\theta\epsilon} + \frac{1}{U-U'}(-4t_e^2 - 2t_at_e) + \frac{1}{(U-U')^2}\times \Big(-t_a^2\,U_{aa\theta\theta} + t_at_e\Big(\frac{6}{5}J + 2U' - 2U_{a\theta a\theta}\Big) + t_e^2\Big(\frac{12}{5}J + 4U' - U_{aa\theta\theta} - 4U_{\theta\theta\epsilon\epsilon} - 4U_{\theta\epsilon\theta\epsilon}\Big)\Big)\Big] \quad (56)$$

In formal octahedral symmetry, the *A* and *E* manifolds are degenerate and split by J_1 and J_2 in the same way. To introduce this artificial spherical symmetry, we impose the same isotropic relations as we used in eq 34. We then indeed immediately verify that the expressions for the J_1 and J_2 parameters become identical for both $^2T_{1g}$ components

$$J_1 = \frac{1}{9}\Big[-6B_{iiii} - 12B_{iijj} + \frac{1}{U-U'}12t^2 + \frac{t^2}{(U-U')^2}\Big(\frac{-216}{5}J - 12U' + 12U_{iiii} + 24U_{iijj}\Big)\Big]$$

$$J_2 = \frac{1}{18}\Big[3B_{iiii} - 3B_{iijj} - \frac{1}{U-U'}6t^2 + \frac{t^2}{(U-U')^2}\Big(\frac{18}{5}J + 6U' - 6U_{iiii} + 6U_{iijj}\Big)\Big] \quad (57)$$

This is a gratifying check of the complicated energy expressions in Table 9. For a discussion of the experimental data and the ab initio calculations for the $Cr_2Cl_9^{3-}$ complex, we return to the expressions for J_1 and J_2 in eqs 55 and 56 for the A and E manifold, respectively.

With the assumptions made above in the discussion of the $^4A_{2g}-^2E_g$ states, the J_1 and J_2 parameters become for the A manifold

$$J_1 = \frac{1}{9}\left[-18B' - \frac{1}{U-U'}4t_a^2 + \frac{1}{(U-U')^2}t_a^2\left(\frac{12}{5}J + 4U' - 4U_{aaaa}\right)\right]$$

$$J_2 = \frac{1}{9}\left[-\frac{1}{U-U'}2t_a^2 + \frac{1}{(U-U')^2}t_a^2 \times \left(\frac{6}{5}J + 2U' - 2U_{aaaa}\right)\right] \quad (58)$$

From the ab initio calculations as well as from experimental evidence, these two parameters are negative and of the same order of magnitude, the difference between averaged single and double prime triplet states, $4J_2$, being a bit smaller in absolute value than the difference between averaged quintet and triplet states, $2J_1$. This can be traced back immediately to the absence of the B' parameter in the expression for J_2. The ratio of the splittings ($^5A_1' - {}^5A_2''$) and ($^3A_1' - {}^3A_2''$) of -3 is very well obeyed at all levels of ab initio calculations; the experimental ratio is approximately -4. Comparing experimental and ab initio results further, one notices that the exact ordering is not the same, the position of the $^5A_2''$ and $^3A_2''$ states being interchanged.

Within the E block, we retain the following expressions for the two parameters

$$J_1 = \frac{1}{9}\left[-18B' + \frac{1}{U-U'}8t_a^2 + \frac{1}{(U-U')^2}t_a^2 \left(\frac{-114}{5}J - 8U' + 8U_{aaaa}\right)\right]$$

$$J_2 = \frac{1}{9}\left[3B' - \frac{1}{U-U'}t_a t_e - \frac{1}{2(U-U')^2}t_a^2 U_{aa\theta\theta}\right] \quad (59)$$

From the experimental data, the position of the ^5E states is not clear, but in any case they are above the triplets. This is confirmed at all levels of ab initio calculations and by our model expressions. These further predict that the averaged prime states are above the averaged double prime states, which is indeed confirmed by the ab initio calculations. The ratio of -3 is very well reproduced.

We now would like to compare the splitting of the E states in the $^4A_{2g}-^2E_g$ and $^4A_{2g}-^2T_{1g}$ manifold, respectively. Since we only have experimental results for $^4A_{2g}-^2E_g$ in $Cr_2Br_9^{3-}$ and for $^4A_{2g}-^2T_{1g}$ in $Cr_2Cl_9^{3-}$, the discussion will be restricted to some qualitative comments. In the expression for J_1, we see immediately that the contribution of $t_a^2/(U - U')$ is doubled in $^4A_{2g}-^2T_{1g}$ with respect to $^4A_{2g}-^2E_g$. Thus, we can say that in $^4A_{2g}-^2T_{1g}$ the splitting between averaged quintets and triplets should be more important than in $^4A_{2g}-^2E_g$, which is indeed confirmed by ab initio calculations and experiment. The expressions for J_2 are more difficult to compare since we only have a rough estimate of the relative importances of the various contributions, by taking the values of the parameters as deduced for $Ti_2Cl_9^{3-}$. The dominant contribution of $t_a t_e/(U - U')$ is now twice as large in $^4A_{2g}-^2E_g$ as compared to $^4A_{2g}-^2T_{1g}$, which is consistent with the ab initio and experimental results.

In summary, a model study of exchange interactions in the $Cr_2Cl_9^{3-}$ system yields several interesting conclusions. The ground-state energy splittings are found to obey a Landé splitting pattern. Although there are claims for a deviation from this interval rule,[51] we find the experimental evidence in favor of the contrary. Due to orbital degeneracy in the excited states, an at first sight very complex splitting pattern is observed. Through thorough inspection of both parametric energy expressions and ab initio and experimental evidence, a simple two-parameter Hamiltonian could be constructed, which elucidates the complex electronic structure of the excited manifold. The underlying symmetry on which this model is based remains as yet hidden.

6. Further Outlook

The idea that bonding between atomic systems can arise via exchange has a respectable history in the study of quantum mechanics. Its application to interactions between bridged transition-metal centers was seriously investigated from the 1970s onward, with the help of a full arsenal of spectroscopic and magnetic techniques involving magnetic circular dichroism, site-selective luminescence, inelastic neutron scattering, oriented electron spin resonance, etc.

At about the same time, several theoretical models were developed, which attempted to extend the succesful spin Hamiltonian formalism to systems with unquenched orbital moments. These models were based on general symmetry considerations and were often scaled with respect to low-resolution quantities such as magnetic susceptibility. At the beginning of the 1990s, attention was attracted to more complex polymetallic systems,[67] which were promising molecular magnets but obviously could not be treated with the same detail as the dimeric systems in view of the multiplicative growth of the eigenspace with the number of magnetic centers.

Only quite recently an opportunity was offered to return to a closer study of the simple exchange systems when ab initio results became available that for the first time described the exchange manifold with sufficient accuracy.[25,31] In this respect, we are certainly entering a new era where correlated ab initio calculations will finally be able to unravel the fine structure of these manifolds. Specially designed methods such as the difference-dedicated configuration interaction (DDCI)[68] bring experimental accuracy within reach. This evolution in our opinion has cleared the scene for more mature models of exchange electronic structure to make a reappearance. This time they can afford to be based on a full microscopic Hamiltonian which is expanded to include all two-body interactions. The many parameters that such an approach generates can be coped with by direct comparison to the ab initio results. The specific role of the models in this case is to bring order

and understanding in the rich fine structure of these spectra. Only through such models can one discover and hopefully understand effects such as the special symmetry which arises when two half-filled shells on metallic neighbors interact.

To some extent, the future of these models is similar to the fate of detailed theories such as the Slater−Condon−Shortley theory of atomic spectra or the ligand-field theory for mononuclear complexes. Although straightforward ab initio treatments are gradually taking over, it is important to remember that in these spectroscopies "the series of experimentally established levels previously classified as components of pure d^q configurations are still there, observable as ever".[69]

7. Acknowledgements

Theoretical research in Leuven is supported by the Concerted Action Scheme of the Flemish Government and by the Fonds voor Wetenschappelijk Onderzoek Vlaanderen. The authors are grateful to H. Weihe for an early draft of ref 8, which contained the treatment of the tetragonal d^1-d^1 case, and to B. Tsukerblat for a preprint of ref 10.

8. Appendix 1

The intercenter two-electron interactions in a trigonal symmetry basis are described by

$$
\begin{aligned}
H_0^{AB} = \sum_{\sigma\sigma'} (&U_{aaaa} n^A_{a\sigma} n^B_{a\sigma'} + U_{\theta\theta\theta\theta}(n^A_{\theta\sigma} n^B_{\theta\sigma'} + n^A_{\epsilon\sigma} n^B_{\epsilon\sigma'} + \\
&n^A_{\theta\sigma} n^B_{\epsilon\sigma'} + n^A_{\epsilon\sigma} n^B_{\theta\sigma'}) + U_{aa\theta\theta}(a^\dagger_{a\sigma} a_{\theta\sigma} b^\dagger_{a\sigma'} b_{\theta\sigma'} + \\
&a^\dagger_{a\sigma} a_{\epsilon\sigma} b^\dagger_{a\sigma'} b_{\epsilon\sigma'} + a^\dagger_{\theta\sigma} a_{a\sigma} b^\dagger_{\theta\sigma'} b_{a\sigma'} + a^\dagger_{\epsilon\sigma} a_{a\sigma} b^\dagger_{\epsilon\sigma'} b_{a\sigma'} + \\
&a^\dagger_{a\sigma} a_{\theta\sigma} b^\dagger_{\theta\sigma'} b_{a\sigma'} + a^\dagger_{a\sigma} a_{\epsilon\sigma} b^\dagger_{\epsilon\sigma'} b_{a\sigma'} + a^\dagger_{\theta\sigma} a_{a\sigma} b^\dagger_{a\sigma'} b_{\theta\sigma'} + \\
&a^\dagger_{\epsilon\sigma} a_{a\sigma} b^\dagger_{a\sigma'} b_{\epsilon\sigma'}) + U_{a\theta a\theta}(n^A_{a\sigma} n^B_{\theta\sigma'} + n^A_{a\sigma} n^B_{\epsilon\sigma'} + n^A_{\theta\sigma} n^B_{a\sigma'} + \\
&n^A_{\epsilon\sigma} n^B_{a\sigma'}) + U_{\theta\theta\epsilon\epsilon}(a^\dagger_{\theta\sigma} a_{\epsilon\sigma} b^\dagger_{\theta\sigma'} b_{\epsilon\sigma'} + a^\dagger_{\epsilon\sigma} a_{\theta\sigma} b^\dagger_{\epsilon\sigma'} b_{\theta\sigma'} + \\
&a^\dagger_{\theta\sigma} a_{\epsilon\sigma} b^\dagger_{\epsilon\sigma'} b_{\theta\sigma'} + a^\dagger_{\epsilon\sigma} a_{\theta\sigma} b^\dagger_{\theta\sigma'} b_{\epsilon\sigma'} - 2n^A_{\theta\sigma} n^B_{\epsilon\sigma'} - 2n^A_{\epsilon\sigma} n^B_{\theta\sigma'})) - \\
&B_{aaaa} \sum_\sigma (n^A_{a\sigma} n^B_{a\sigma} + a^\dagger_{a\sigma} a_{a-\sigma} b^\dagger_{a-\sigma} b_{a\sigma}) - \\
&B_{\theta\theta\theta\theta}(\sum_\sigma (n^A_{\theta\sigma} n^B_{\theta\sigma} + a^\dagger_{\theta\sigma} a_{\theta-\sigma} b^\dagger_{\theta-\sigma} b_{\theta\sigma} + n^A_{\epsilon\sigma} n^B_{\epsilon\sigma} + \\
&a^\dagger_{\epsilon\sigma} a_{\epsilon-\sigma} b^\dagger_{\epsilon-\sigma} b_{\epsilon\sigma}) + \sum_{\sigma\sigma'} (a^\dagger_{\theta\sigma} a_{\epsilon\sigma'} b^\dagger_{\epsilon\sigma'} b_{\theta\sigma} + a^\dagger_{\epsilon\sigma} a_{\theta\sigma'} b^\dagger_{\theta\sigma'} b_{\epsilon\sigma})) - \\
&B_{a\theta\theta a}(\sum_\sigma (n^A_{a\sigma} n^B_{\theta\sigma} + a^\dagger_{a\sigma} a_{a-\sigma} b^\dagger_{\theta-\sigma} b_{\theta\sigma} + n^A_{a\sigma} n^B_{\epsilon\sigma} + \\
&a^\dagger_{a\sigma} a_{a-\sigma} b^\dagger_{\epsilon-\sigma} b_{\epsilon\sigma} + n^A_{\theta\sigma} n^B_{a\sigma} + a^\dagger_{\theta\sigma} a_{\theta-\sigma} b^\dagger_{a-\sigma} b_{a\sigma} + n^A_{\epsilon\sigma} n^B_{a\sigma} + \\
&a^\dagger_{\epsilon\sigma} a_{\epsilon-\sigma} b^\dagger_{a-\sigma} b_{a\sigma}) - B_{aa\theta\theta} \sum_{\sigma\sigma'} (a^\dagger_{a\sigma} a_{\theta\sigma'} b^\dagger_{a\sigma'} b_{\theta\sigma} + \\
&a^\dagger_{a\sigma} a_{\epsilon\sigma'} b^\dagger_{a\sigma'} b_{\epsilon\sigma} + a^\dagger_{\theta\sigma} a_{a\sigma'} b^\dagger_{\theta\sigma'} b_{a\sigma} + a^\dagger_{\epsilon\sigma} a_{a\sigma'} b^\dagger_{\epsilon\sigma'} b_{a\sigma}) - \\
&B_{a\theta a\theta} \sum_{\sigma\sigma'} (a^\dagger_{a\sigma} a_{\theta\sigma'} b^\dagger_{\theta\sigma'} b_{a\sigma} + a^\dagger_{a\sigma} a_{\epsilon\sigma'} b^\dagger_{\epsilon\sigma'} b_{a\sigma} + \\
&a^\dagger_{\theta\sigma} a_{a\sigma'} b^\dagger_{a\sigma'} b_{\theta\sigma} + a^\dagger_{\epsilon\sigma} a_{a\sigma'} b^\dagger_{a\sigma'} b_{\epsilon\sigma}) - B_{\theta\epsilon\epsilon\theta}(\sum_\sigma (n^A_{\theta\sigma} n^B_{\epsilon\sigma} + \\
&a^\dagger_{\theta\sigma} a_{\theta-\sigma} b^\dagger_{\epsilon-\sigma} b_{\epsilon\sigma} + n^A_{\epsilon\sigma} n^B_{\theta\sigma} + a^\dagger_{\epsilon\sigma} a_{\epsilon-\sigma} b^\dagger_{\theta-\sigma} b_{\theta\sigma}) - \\
&\sum_{\sigma\sigma'} (a^\dagger_{\theta\sigma} a_{\epsilon\sigma'} b^\dagger_{\epsilon\sigma'} b_{\theta\sigma} + a^\dagger_{\epsilon\sigma} a_{\theta\sigma'} b^\dagger_{\theta\sigma'} b_{\epsilon\sigma})) - \\
&B_{\theta\theta\epsilon\epsilon} \sum_{\sigma\sigma'} (a^\dagger_{\theta\sigma} a_{\epsilon\sigma'} b^\dagger_{\theta\sigma'} b_{\epsilon\sigma} + a^\dagger_{\epsilon\sigma} a_{\theta\sigma'} b^\dagger_{\epsilon\sigma'} b_{\theta\sigma} - a^\dagger_{\theta\sigma} a_{\epsilon\sigma'} b^\dagger_{\epsilon\sigma'} b_{\theta\sigma} - \\
&a^\dagger_{\epsilon\sigma} a_{\theta\sigma'} b^\dagger_{\theta\sigma'} b_{\epsilon\sigma}) \quad (60)
\end{aligned}
$$

This expression incorporates the following trigonal symmetry relations

$$
\begin{aligned}
U_{\theta\theta\theta\theta} &= 2U_{\theta\theta\epsilon\epsilon} + U_{\theta\epsilon\theta\epsilon} \\
B_{\theta\theta\theta\theta} &= B_{\theta\theta\epsilon\epsilon} + B_{\theta\epsilon\epsilon\theta} + B_{\theta\epsilon\theta\epsilon} \qquad (61)
\end{aligned}
$$

In our original paper, we proposed a simplified version of this Hamiltonian with $B_{aa\theta\theta} = B_{a\theta\theta a}$ and $B_{\theta\theta\epsilon\epsilon} = B_{\theta\epsilon\epsilon\theta}$. These equalities strictly hold in the spherical symmetry limit only and have therefore not been introduced in the present expressions.

9. References

(1) Kahn, O. *Molecular Magnetism*; VCH: New York, 1993.
(2) *Magnetic Molecular Materials*; Gatteschi, D., Kahn, O., Miller, J. S., Palacio, F., Eds.; NATO ASI Series E, 1991; Vol. 198.
(3) Gatteschi, D. *Adv. Mater.* **1994**, *6*, 635.
(4) Miller, J. S.; Epstein, A. J. *Adv. Chem. Ser.* **1995**, *245*, 161.
(5) Miller, J. S.; Epstein, A. J. *Chem. Eng. News* **1995**, Oct. 2, 30.
(6) Kollmar, C; Kahn, O. *Acc. Chem. Res.* **1993**, *26*, 259.
(7) Drillon, M.; Darrier, J. *Struct. Bonding* **1992**, *79*, 55.
(8) Weihe, H; Güdel, H. U. *Chem. Phys. Lett.* **1996**, *261*, 123.
(9) Borrás-Almenar, J. J.; Clemente-Juan, J. M.; Coronado, E.; Palii, A. V.; Tsukerblat, B. S. *J. Phys. Chem.* **1998**, *A102*, 200.
(10) Borrás-Almenar, J. J.; Clemente-Juan, J. M.; Coronado, E.; Palii, A. V.; Tsukerblat, B. S. Manuscript in preparation.
(11) Anderson, P. W. *Phys. Rev.* **1959**, *115*, 2.
(12) Anderson, P. W. In *Solid State Physics*; Seitz, F., Turnbull, D., Eds.; Academic Press: New York, 1963; Vol. 14, p 99.
(13) Griffith, J. S. *The Theory of Transition-Metal Ions*; Cambridge University Press: Cambridge, 1961; p 361.
(14) Delfs, C. D.; Gatteschi, D.; Pardi, L. *Comments Inorg. Chem.* **1993**, *15*, 27.
(15) Slater, J. C. *Quantum Theory of Molecules and Solids*; McGraw-Hill: New York, 1974; Vol. IV.
(16) Judd, B. R. *Second Quantization and Atomic Spectroscopy*; The John Hopkins Press: Baltimore, 1967.
(17) Heisenberg, W. *Z. Phys.* **1928**, *49*, 619.
(18) Davydov, A. S. *Quantum Mechanics*; Pergamon: Oxford, 1976.
(19) Dirac, P. A. M. *The Principles of Quantum Mechanics*, 4th ed.; Oxford University Press: New York, 1958; p 222.
(20) Ferguson, J.; Guggenheim, H. J.; Tanabe, Y. *J. Phys. Soc. Jpn.* **1966**, *21*, 692.
(21) Kahn, O. *Mol. Phys.* **1975**, *29*, 1039.
(22) Weihe, H.; Güdel, H. U. *Inorg. Chem.* **1997**, *36*, 3632.
(23) Weihe, H.; Güdel, H. U. *J. Am. Chem. Soc.* **1997**, *119*, 6539.
(24) Weihe, H.; Güdel, H. U. *J. Am. Chem. Soc.* **1998**, *120*, 2870.
(25) Fink, K.; Fink, R.; Staemmler, V. *Inorg. Chem.* **1994**, *33*, 6219.
(26) Hay, P. J.; Thibeault, J. C.; Hoffmann, R. *J. Am. Chem. Soc.* **1975**, *97*, 4884.
(27) Van Kalkeren, G.; Schmidt, W. W.; Block, R. *Physica* **1979**, *97B*, 315.
(28) Kahn, O. *Mol. Phys.* **1976**, *31*, 957.
(29) Briat, B.; Kahn, O.; Morgenstern-Badarau, I.; Rivoal, J. C. *Inorg. Chem.* **1981**, *20*, 4193.
(30) Leuenberger, B.; Güdel, H. U. *Mol. Phys.* **1984**, *51*, 1.
(31) Ceulemans, A.; Heylen, G. A.; Chibotaru, L. F.; Maes, T. L.; Pierloot, K.; Ribbing, C.; Vanquickenborne, L. G. *Inorg. Chim. Acta* **1996**, *251*, 15.
(32) Ceulemans, A.; Bongaerts, N.; Vanquickenborne, L.G. *Inorg. Chem.* **1987**, *26*, 1566.
(33) Dionne, G. F.; Palm, B. J. *J. Magn. Reson.* **1986**, *68*, 355.
(34) Barraclough, C. G.; Gregson, A. K. *J. Chem. Soc., Faraday Trans.* II **1972**, 177.
(35) Ceulemans, A.; Chibotaru, L. F.; Heylen, G. A.; Pierloot, K. *Mol. Phys.* **1999**, *97*, 1197.
(36) Hoffmann, R. *Acc. Chem. Res.* **1971**, *4*, 1.
(37) Glerup, J. *Acta Chem. Scand.* **1972**, *26*, 3775.
(38) Atanasov, M. A.; Schmidtke, H.-H. *Chem. Phys.* **1988**, *123*, 205.
(39) Drillon, M.; Georges, R. *Phys. Rev.* **1982**, *B26*, 3882.
(40) Ballhausen, C. J. *Introduction to Ligand Field Theory*; McGraw Hill: New York, 1962; p 89.
(41) Condon, E. U.; Odabaşi, H. *Atomic Structure*; Cambridge University Press: Cambridge, 1980; p 235.
(42) Cotton, F. A.; Feng, X.; Gütlich, P.; Kohlhaels, T.; Shang, J. L. *Inorg. Chem.* **1994**, *33*, 3055.
(43) Leuenberger, B.; Güdel, H. U.; Furrer, A. *Chem. Phys. Lett.* **1986**, *126*, 255.
(44) Ceulemans, A. In *Vibronic Processes in Inorganic Chemistry*; Flint, C. D., Ed.; NATO ASI Series C; Kluwer Academic Publishers: New York, 1989, Vol. 282, pp 221−254.

(45) Taken from Heylen, G. *Theoretical Analysis of Exchange Interactions in Face-Sharing Bioctahedral Complexes of Ti(III), Cr(III), and Co(II)*; Ph.D. Thesis, University of Leuven, 1999.
(46) Kahn, O.; Briat, B. *Chem. Phys. Lett.* **1975**, *32*, 376.
(47) Briat, B.; Russel, M. F.; Rivoal, J. C.; Chapelle, J. P.; Kahn, O. *Mol. Phys.* **1977**, *34*, 1357.
(48) Johnstone, I. W.; Maxwell, K. J.; Stevens, K. W. H. *J. Phys. C: Solid State Phys.* **1981**, *14*, 1297.
(49) Leuenberger, B.; Güdel, H. U.; Kjems, J. K.; Petitgrand, D. *Inorg. Chem.* **1985**, *24*, 1035.
(50) Beswick, J. R.; Dugdale, D. E. *J. Phys. C: Solid State Phys.* **1973**, *6*, 3326.
(51) Benson, P. C.; Dugdale, E. C. *J. Phys. C: Solid State Phys.* **1975**, *8*, 3872.
(52) Dubicki, L.; Ferguson, J.; Harrowfield, B. V. *Mol. Phys.* **1977**, *34*, 1545.
(53) Leuenberger, B.; Güdel, H. U.; Feile, R.; Kjems, J. K. *Phys. Rev.* **1983**, *B28*, 5368.
(54) Leuenberger, B.; Stebler, A.; Güdel, H. U.; Furrer, A.; Feile, R.; Kjems, J. K. *Phys. Rev.* **1984**, *B30*, 6300.
(55) Wieghardt, K.; Chaudhuri, P.; Nuber, B.; Weiss, J. *Inorg. Chem.* **1982**, 21.
(56) Bolster, D. E.; Gütlich, P.; Hatfield, W. E.; Kremer, S.; Müller, E. W.; Wieghardt, K. *Inorg. Chem.* **1983**, *22*, 1725.
(57) Riesen, H.; Güdel, H. U.; Chaudhuri, P.; Wieghardt, K. *Chem. Phys. Lett.* **1984**, *110*, 552.
(58) Riesen, H.; Reber, C.; Güdel, H. U.; Wieghardt, K. *Inorg. Chem.* **1987**, *26*, 2747.
(59) Riesen, H.; Güdel, H. U. *J. Chem. Phys.* **1987**, *87*, 3166.
(60) Glerup, J.; Larsen, S.; Weihe, H. *Acta Chem. Scand.* **1993**, *47*, 1154.
(61) Leuenberger, B.; Güdel, H. U. *Inorg. Chem.* **1986**, *25*, 181.
(62) Dubicki, L.; Tanabe, Y. *Mol. Phys.* **1977**, *34*, 1531.
(63) Barry, K. R.; Maxwell, K. J.; Siddiqui, K. A.; Stevens, K. W. H. *J. Phys. C: Solid State Phys.* **1981**, *14*, 1281.
(64) Ceulemans, A. *Top. Curr. Chem.* **1994**, *171*, 27.
(65) Schenker, R.; Weihe, H.; Güdel, H. U. *XXXIII Int. Conf. Coord. Chem.*, Florence, Aug. 30−Sept. 4, 1998, Book of Abstracts, p 710.
(66) Riesen, H.; Güdel, H. U. *Mol. Phys.* **1987**, *60*, 1221.
(67) Caneschi, A.; Gatteschi, D.; Pardi, L.; Sessoli, R. *Perspec. Coord. Chem.* **1992**, 109.
(68) Miralles, J.; Castell, O.; Caballol, R.; Malrieu, J. P. *Chem. Phys.* **1993**, *172*, 33.
(69) Bendix, J.; Brorson, M.; Schaffer, C. E. *Inorg. Chem.* **1993**, *32*, 2838.

CR960129K